



Published in final edited form as:

*J Med Chem.* 2013 June 27; 56(12): 4990–5008. doi:10.1021/jm400248c.

## A potent and selective small molecule inhibitor for the lymphoid-specific tyrosine phosphatase (LYP), a target associated with autoimmune diseases

Yantao He<sup>#,‡</sup>, Sijiu Liu<sup>#,‡</sup>, Ambili Menon<sup>Φ</sup>, Stephanie Stanford<sup>+</sup>, Emmanuel Oppong<sup>Φ</sup>, Andrea M. Gunawan<sup>#</sup>, Li Wu<sup>#</sup>, Dennis J. Wu<sup>+</sup>, Amy M. Barrios<sup>||</sup>, Nunzio Bottini<sup>+</sup>, Andrew C. B. Cato<sup>Φ</sup>, and Zhong-Yin Zhang<sup>#,\*</sup>

<sup>#</sup>Department of Biochemistry and Molecular Biology, Indiana University School of Medicine, 635 Barnhill Drive, Indianapolis, Indiana 46202, USA

<sup>Φ</sup>Karlsruhe Institute of Technology, Institute of Toxicology and Genetics, Hermann-von-Helmholtz-Platz 1, 76344 Eggenstein-Leopoldshafen, Germany

<sup>+</sup>Division of Cellular Biology, La Jolla Institute for Allergy and Immunology, 9420 Athena Circle, La Jolla, CA 92037, USA

<sup>||</sup>Department of Medicinal Chemistry, University of Utah, Salt Lake City, UT 84112, USA

### Abstract

Lymphoid-specific tyrosine phosphatase (LYP), a member of the protein tyrosine phosphatase (PTP) family of signaling enzymes, is associated with a broad spectrum of autoimmune diseases. Herein we describe our structure-based lead optimization efforts within a 6-hydroxy-benzofuran-5-carboxylic acid series culminating in the identification of compound **8b**, a potent and selective inhibitor of LYP with a  $K_i$  value of 110 nM and more than 9-fold selectivity over a large panel of PTPs. The structure of LYP in complex with **8b** was obtained by X-ray crystallography, providing detailed information about the molecular recognition of small-molecule ligands binding LYP. Importantly, compound **8b** possesses highly efficacious cellular activity in both T- and mast cells and is capable of blocking anaphylaxis in mice. Discovery of **8b** establishes a starting point for the development of clinically useful LYP inhibitors for treating a wide range of autoimmune disorders.

### Introduction

Protein tyrosine phosphorylation is critical for the control of cellular processes such as proliferation, differentiation, metabolism and survival, as well as immune responses.<sup>1</sup> Proper levels of tyrosine phosphorylation, regulated by the reciprocal action of protein tyrosine kinases (PTKs) and protein tyrosine phosphatases (PTPs), define the signaling threshold for a given stimulus and are critical for normal physiology and development. Consequently, alterations in the expression or activity of PTKs as well as PTPs can have dire pathophysiological consequences. Indeed, defects in tyrosine phosphorylation-mediated signaling events are associated with many human diseases including cancer, diabetes/obesity, and autoimmune disorders.<sup>1,2</sup> More than a dozen drugs targeting PTKs have been approved for clinical use over the past decade, and many more are undergoing clinical

\*Corresponding Author: To whom correspondence should be addressed. Phone: (317) 274-8025; fax: (317) 274-4686; zyzhang@iu.edu.

<sup>‡</sup>Author Contributions: These authors contributed equally to this work.

trials.<sup>3</sup> However, the therapeutic potential of modulating the PTPs is still underexplored despite the fact that several PTPs have been identified as high value targets.<sup>4,5</sup>

Genetic studies in human autoimmunity have brought lymphoid-specific tyrosine phosphatase (LYP) to the spotlight. LYP is expressed exclusively in immune cells<sup>6</sup> and functions as a negative regulator of T cell receptor (TCR) signaling pathways, likely through dephosphorylation of the Lck and ZAP-70 kinases.<sup>7-9</sup> A missense C1858T single nucleotide polymorphism in the gene encoding LYP, *PTPN22*, was found to be a common risk factor for multiple autoimmune disorders, including type I diabetes,<sup>10</sup> rheumatoid arthritis,<sup>11,12</sup> Graves disease,<sup>13</sup> systemic lupus erythematosus,<sup>14</sup> myasthenia gravis,<sup>15,16</sup> and generalized vitiligo.<sup>17,18</sup> In fact, the *PTPN22* locus is one of the strongest risk factors outside of the major histocompatibility complex that associates with autoimmune diseases.<sup>19</sup> The C1858T variation converts an Arg at position 620 into a Trp within the first Pro-rich region in the C-terminus of LYP, diminishing the ability of LYP to bind to the SH3 domain of the Src C-terminal kinase (Csk).<sup>10,11</sup> Importantly, this autoimmune-predisposing LYP-W620 variant is a gain-of-function form of the phosphatase, rendering increased inhibition of T- and B-cell signaling compared to the wild-type enzyme.<sup>20-24</sup> Interestingly, a loss-of-function LYP variant is linked to reduced risk of systemic lupus erythematosus.<sup>25</sup> A more recent report indicated that LYP plays an important role in T<sub>reg</sub> generation and function, and mice lacking LYP show improved immunosuppressive responses.<sup>26</sup> Moreover, inducible LYP knockdown in non-obese diabetic mice conferred protection from type 1 diabetes.<sup>27</sup> Taken together, these data establish LYP as an exciting target for pharmacological intervention of a broad spectrum of autoimmune disorders.

Given the strong linkage of LYP to autoimmunity, there is increasing interest in developing LYP-based small molecule therapeutics.<sup>24, 28-35</sup> Unfortunately, most of the existing LYP inhibitors lack the required potency, selectivity, and/or *in vivo* efficacy for clinical evaluation. Indeed, PTP-based drug discovery programs have historically been shrouded with difficulty in inhibitor selectivity and bioavailability, both of which stem from the intrinsic properties of the PTP active site. The pTyr binding pocket, which represents the PTP active site, is highly conserved, so achieving PTP inhibitor selectivity is extremely challenging. Moreover, the PTP active site is also positively charged, so brute-force compound screening campaigns usually lead to the identification of negatively charged molecules that do not readily penetrate cell membranes. Since a disproportionately high percentage of FDA-approved drugs originate from natural products, we have focused our effort to search for natural product-like PTP inhibitory agents. We discovered that bicyclic salicylates can serve as effective nonhydrolyzable pTyr mimics and are sufficiently polar to bind the PTP active site, yet remain capable of efficiently crossing cell membranes.<sup>36</sup> One effective strategy to enhance PTP inhibitor potency and selectivity has been to link appropriately functionalized diversity elements to a nonhydrolyzable pTyr mimetic in order to engage less conserved interactions outside of the pTyr-binding cleft.<sup>37,38</sup> We describe here a structure-based focused library approach that transforms the 6-hydroxy-benzofuran-5-carboxylic acid Core **1** (Figure 1) into the highly potent and selective LYP inhibitor compound **8b**, which has efficacious activity in both cells and live animals. X-ray crystallographic analysis of the structure of LYP in complex with compound **8b** reveals detailed information about the molecular recognition of small-molecule inhibitors binding LYP. This compound represents an excellent starting point for the development of clinically useful LYP inhibitors for the treatment of a wide variety of autoimmune diseases.

## Results

### Development of a potent and selective LYP inhibitor based on the 6-hydroxy-benzofuran-5-carboxylic acid core 1

Our initial effort in LYP inhibitor discovery involved the use of Click chemistry to tether 80 azide-containing amines to an alkyne-containing 6-hydroxy-benzofuran-5-carboxylic acid scaffold (Core **1**) aimed to target secondary binding pockets in the vicinity of the PTP active site. This led to the identification of compound **2**<sup>28</sup> (Figure 1) as a reversible and competitive LYP inhibitor. However, despite the highly efficacious cellular activity, the potency ( $IC_{50} = 4.6 \pm 0.4 \mu\text{M}$ ) and selectivity (2.6-fold against PTP1B and >7-fold against SHP2, HePTP, PTP-Meg2, FAP1, CD45, LAR, PTP $\alpha$ , and VHR) displayed by **2** are relatively modest, and therefore not adequate for chemical biological investigation and therapeutic development.

To guide the development of next generation LYP inhibitors, we solved the structure of LYP in complex with compound **2**.<sup>28</sup> The co-crystal structure reveals that compound **2** binds the LYP active site with the 6-hydroxy-benzofuran-5-carboxylic acid situated in the catalytic site, making a number of hydrogen bonds with the main chain amide of Ala229, the side chains of Cys227 and Cys129, and charge-charge interactions with Arg233 and Lys138, as well as aromatic stacking interactions with Tyr60 and Van der Waals contacts with the aliphatic side chains of Gln274, Ser228, Ala229, and Lys138. In addition, the distal naphthalene ring in **2** occupies a unique peripheral site defined by Phe28, Leu29, and Arg33, which form a pocket equivalent to the second aryl phosphate-binding site previously identified in PTP1B.<sup>37</sup> Unfortunately, the phenyl ring attached to the 2-position of the benzofuran core (Figure 1) was not resolved in the structure, likely due to flexibility as a result of weak interaction with LYP. Additionally, no significant contact was observed between the triazolidine ring linker and LYP. Based on these structural findings and chemical tractability, we devised a molecular hybridization and parallel synthesis strategy to modify the phenyl ring at the 2-position and the alkyne group at the 3-position (Figure 1) of the benzofuran core in order to enhance binding interactions with LYP. This entails (1) modification of the 2-phenyl ring of the benzofuran scaffold to generate compounds **3a–e**, (2) introduction of different aryl substituents to the 3-ethynyl of benzofuran scaffold to create **4a–i**, and (3) combination of the top hits from both **3a–e** and **4a–i** to generate **5a** (Figure 1).

We first sought to optimize the activity of Core **1** for LYP through introduction of different substituents in the 2-phenyl ring. As outlined in Scheme 1, the key intermediate **12** was prepared by a reported procedure.<sup>39</sup> Compound **12** was coupled with appropriate alkynes by Sonogashira reaction to produce **13a–e**, which were cyclized in the presence of  $\text{I}_2$ , yielding 6-iodo-7-(substituted-phenyl)-2,2-dimethyl-4H-[1,3]dioxino[5,4-f]benzofuran-4-one **14a–e**. Subsequently, the replacement of the iodo group of **14a–e** by the acetylene group produced **15a–e**, which upon hydrolysis were transformed to the corresponding 2-(substituted-phenyl)-3-ethynyl-6-hydroxybenzofuran-5-carboxylic acid **3a–e**. The ability of the compounds to inhibit LYP-catalyzed hydrolysis of the chromogenic substrate *p*-nitrophenyl phosphate (*p*NPP) was evaluated at pH 7 and 25 °C. As shown in Table 1, the inhibitory potency of compounds **3a–e** improved 5 to 27.5 fold compared to the starting Core **1** ( $IC_{50} = 50 \mu\text{M}$ ). Selectivity profiling indicated that only compound **3d** exhibited a moderate selectivity (2- to 10 fold) against a number of human PTPs (data not shown). Meanwhile, through a concurrent program to increase interaction between the enzyme and inhibitory agents, substituents were attached to the 3-position of the benzofuran scaffold. We synthesized compounds **4a–i** by coupling appropriate aryl acetylenes to this position (Scheme 2). Compounds **4a–i** were also prepared from compound **12** as reported in our

previous work.<sup>39</sup> These compounds were assayed for LYP inhibition, leading to the identification of LYP inhibitors **4c** ( $IC_{50} = 1.0 \mu\text{M}$ ) and **4i** ( $IC_{50} = 0.63 \mu\text{M}$ ) (Table 2), which are 50-fold more potent than the original lead compound Core **1**. Results from selectivity profiling showed that compound **4c** had better selectivity than **4i** (data not shown). We then hypothesized that merging compound **3d** and **4c** into one structure might further improve potency and selectivity (Figure 1). With this in mind, we synthesized the hybrid inhibitor **5a** ( $IC_{50} = 0.68 \mu\text{M}$ ), as well as three analogues (**5b–d**) of **5a** (Scheme 3). Unfortunately, these compounds exhibited only minor improvement in  $IC_{50}$  values compared to the parent compounds **3d** or **4c** (Table 3). No significant increase in selectivity was observed for the hybrid compounds (data not shown).

To further improve the potency and selectivity of compound **5a**, we embarked on a focused library approach to introduce molecular diversity at the 2-phenyl ring in order to capture additional interactions with LYP. This strategy was based on the limited but promising SAR on the 2-phenyl ring (compound **3** series), which suggests that a more thorough exploration of the substitutions in the 2-phenyl ring of **5a** may lead to the identification improved LYP inhibitory agents. To this end, substituted acetic acid was introduced to either the meta- or para-position of the 2-phenyl ring to generate compounds **6a** and **6b** (Scheme 4). The starting methyl 2-(3-ethynylphenoxy)acetate **23** and methyl 2-(4-ethynylphenoxy)acetate **27**, obtained from 3-iodophenol and 4-iodophenol, were coupled with compound **12** in DMF to afford methyl 2-(3-((7-methoxy-2,2-dimethyl-4-oxo-4H-benzo[d][1,3]dioxin-6-yl)ethynyl)phenoxy)acetate **28** and methyl 2-(4-((7-methoxy-2,2-dimethyl-4-oxo-4H-benzo[d][1,3]dioxin-6-yl)ethynyl)phenoxy)acetate **31**. Synthesis of target compounds **6a** and **6b** utilized compounds **28** and **31** as starting materials in a procedure similar to that developed for preparing **4a–i**.<sup>39</sup> Compounds **6a** and **6b** inhibited LYP with  $IC_{50}$  values of 15 and 7.8  $\mu\text{M}$ , respectively. The decrease in binding affinity for **6a** and **6b** might be caused by the negative charge introduced into the 2-phenyl ring and elimination of the charge through amide condensation reaction could increase binding potency. Thus, compounds **6a** and **6b** were combined with a structurally diverse set of 48 commercially available amines through well-established amide chemistry to create library 7 and library 8 (Figure 2) in order to target sub-pockets that border the active site. These two libraries were screened for inhibition of LYP-catalyzed hydrolysis of *p*NPP at pH 7 and 25 °C. On the basis of our screening data, compounds with para-substituted amides from library 8 are more potent than those with meta-substituted amides from library 7. Compound potency appears to be driven by the hydrophobic character of the amide substituents. The top 8 hits identified from screening were re-synthesized, purified, and their  $IC_{50}$  values were determined. As shown in Table 4, compounds **8a** and **8b** are most potent for LYP with  $IC_{50}$  values of  $0.171 \pm 0.004$  and  $0.259 \pm 0.007 \mu\text{M}$ , respectively. To determine the specificity of compounds **8a** and **8b** for LYP, their inhibitory activity toward a panel of mammalian PTPs including cytosolic PTPs, PTP1B, SHP1, SHP2, TC-PTP, HePTP, PTP-Meg2, PTP-PEST, FAP1, and PTPH1, the receptor-like PTPs, CD45, LAR, PTP $\alpha$ , PTP $\beta$ , PTP $\epsilon$ , PTP $\gamma$ , PTP $\mu$ , and PTP $\sigma$ , the dual specificity phosphatases Laforin, VHR, VHX, VHZ, MKP3, and Cdc14, and the low molecular weight PTP were measured. As shown in Table 5, the selectivity of compound **8b** is superior to **8a**. Compound **8b** exhibits at least 9-fold selectivity for LYP over all PTPs examined.

To further characterize compound **8b** as a LYP inhibitor, its  $IC_{50}$  value was determined under two different conditions: 1) **8b** was pre-mixed with *p*NPP, and the reaction was initiated by the addition of LYP; and 2) **8b** was pre-mixed with the enzyme for 30 minutes, and the reaction was initialized by the addition of *p*NPP. Irreversible, promiscuous nonspecific, or tight-binding inhibitors would be expected to exhibit significantly reduced  $IC_{50}$  values when they are pre-incubated with the enzyme. Similar  $IC_{50}$  values were

obtained for compound **8b** under these two conditions (**8b** pre-mixed with *p*NPP,  $IC_{50} = 0.259 \pm 0.007 \mu\text{M}$ ; **8b** pre-mixed with the enzyme,  $IC_{50} = 0.250 \pm 0.02 \mu\text{M}$ ), suggesting that LYP inhibition by **8b** is reversible. Detailed kinetic analyses revealed that **8b** is a competitive inhibitor for LYP with a  $K_i$  of  $110 \pm 3 \text{ nM}$  (Figure 3). Thus, **8b** represents the most potent and selective LYP inhibitor reported to date.

### Structural basis of LYP inhibition by compound **8b**

To determine the structural basis for LYP inhibition by compound **8b**, we crystallized the PTP domain of LYP (residues 1–303) with **8b**. The three dimensional structure of LYP•**8b** was solved by molecular replacement using the coordinates of LYP apo form (PDB entry code: 2P6X)<sup>40</sup> as a search model and refined to 2.30 Å resolution. The details of the crystals and structure solution are summarized in Table 6. Unambiguous electron densities were observed for compound **8b** in the LYP active site as shown by the unbiased  $F_o - F_c$  difference Fourier maps contoured at  $3.0\sigma$  (Fig. 4A). Similar to other reported PTP structures, the LYP catalytic domain adopts a structure comprising a central eight  $\beta$ -stranded sheet surrounded by six  $\alpha$ -helices on one side and two  $\alpha$ -helices on the other (Figure 4A). The PTP signature motif (H<sup>226</sup>CSAGCGR<sup>233</sup>) forms a loop (P-loop, colored in blue in Figure 4A) at the base of the active-site pocket. The overall structure of LYP•**8b** is quite similar with the initial search model used for molecular replacement.

Consistent with the ability of salicylic acid derivatives to serve as effective pTyr surrogates<sup>28,41–43</sup> and the observed competitive mode of LYP inhibition by **8b**, the 6-hydroxy-benzofuran-5-carboxylic acid moiety is found in the LYP active-site pocket. Interestingly, **8b** targets an inactive LYP conformation because the WPD loop (residues 193–204), which harbors the general acid-base catalyst Asp195, is fully open in the LYP•**8b** structure (colored in green in Figure 4A). The remarkable potency and selectivity of **8b** for LYP are the results of numerous specific interactions with both the active site and its nearby peripheral pockets (Figure 4B). The 6-hydroxy-benzofuran-5-carboxylate is engaged in both polar and hydrophobic interactions with the LYP active site. The carboxylate in **8b** forms hydrogen bonds with the main-chain amide of Arg233, the side chains of Arg233 and Gln278, and a charge-charge interaction with the main-chain oxygen of Cys231. The adjacent hydroxyl group in 6-hydroxy-benzofuran-5-carboxylic acid makes three additional hydrogen bonds with the main-chain amides of Ser228 and Ala229 as well as the side-chain of Arg233, which further strengthens its polar interactions with the active site. In addition to the polar interactions, the benzofuran ring participates in hydrophobic interactions with Tyr60 in the pTyr recognition loop (residues 58–63) and Van der Waals contacts with the aliphatic side chains of Gln274 in the Q-loop (residues 269–278), and Ala229 and Ser228 in the P-loop. Besides interactions within the LYP active site, the phenyl ring connected to the 2-position of the benzofuran core makes aromatic–aromatic stacking interactions with Tyr60 in the pTyr recognition loop and Van der Waals contacts with side chain atoms (C $\gamma$ , O $\delta_1$ , and O $\delta_2$ ) of Asp62. In addition, the distal cyclopropanamide in **8b** also interacts with the pTyr recognition loop by contributing H-bonds with the main-chain amides of Lys61 and Asp62, donating a charge-charge interaction with the side chain of Asp62, and making hydrophobic contacts with the side chains of Tyr60, Lys61 and Asp62 (Figure 4B). This binding site is equivalent to the –1 binding pocket previously identified in the PTP1B-phosphopeptide structures.<sup>44</sup> Given the hydrophobic nature of this binding site, it is not surprising that compounds **8a–g** have comparable  $IC_{50}$  values against LYP (Table 4), indicating that they inhibit LYP with a similar binding mode. The LYP•**8b** structure also provides insight into why the affinity of **6b** is lower than that of **5a**, likely due to an electrostatic repulsion between the carboxylate in the 2-phenyl ring and the side-chain of Asp62 (the distance between the two carboxylate groups is 3 Å). Finally, the 3-chlorophenyl ring attached to the 3-ethynyl group participates in Van der Waals interactions with the

aliphatic side chains of Gln274 and Thr275 in the Q-loop. The chlorine atom may also make Van der Waals contacts with the side chains of Lys32 and Phe28, which are close to a LYP-specific insert (residues 35–42).

Although both compounds **8b** and **2** bind to the active site of LYP, their binding modes are quite different. Compared to **8b**, the benzofuran moiety in **2** rotates 100° anti-clockwise and shifts 2.4 Å to the right (Figure 4C). Superposition of the LYP•**8b** and LYP•**2** structures reveals that the 6-hydroxy-benzofuran-5-carboxylate in **8b** extends deeper into the LYP active site. The carboxylate in **2** is located at the same position of the hydroxyl group in **8b**. Thus the 6-hydroxy-benzofuran-5-carboxylate moiety in **8b** experiences more and stronger polar and hydrophobic interactions with the LYP active site than that in **2**. For example, the salicylate in **8b** is engaged in 9 polar interactions with the LYP active site, while only 6 polar interactions are found in the LYP•**2** structure.<sup>28</sup> Most of the Van der Waals contact distances between the benzofuran core in **8b** and LYP residues are within 4 Å, while in the LYP•**2** structure, these distances are longer than 4.0 Å. Furthermore, the substituted phenyl group at the 2-position of the benzofuran ring in **8b** makes extensive hydrophobic interactions with the pTyr recognition loop, while the corresponding phenyl ring in **2** is invisible in the co-crystal structure. These increased and stronger interactions between **8b** and LYP are consistent with the 26.6-fold increase in binding affinity for **8b** ( $K_i = 2.9 \mu\text{M}$  for **2**).

### Compound **8b** increases T cell activation

Given the excellent potency and selectivity of **8b** for LYP, we proceeded to evaluate the ability of **8b** to inhibit LYP inside the cell. As LYP acts as a potent inhibitor of signaling through the T cell receptor (TCR),<sup>45</sup> we first tested the effect of the compound on early TCR signaling in JTAG cells, a human T cell line. As shown in Figure 5A, treatment of JTAG cells with 15  $\mu\text{M}$  **8b** increased both basal and TCR-stimulated phosphorylation of ZAP-70 on Tyr319. Given the increased activation of ZAP-70 in resting cells, we next tested whether the compound induces downstream activation of T cells, as assessed by surface expression of CD69, a marker of T cell activation.<sup>46</sup> As shown in Figure 5B, treatment of JTAG cells with 15  $\mu\text{M}$  **8b** led to increased expression of CD69 in resting JTAG cells. We next sought to determine whether **8b** inhibits PEP, the mouse ortholog of LYP, in primary mouse T cells, by determining the effect of the compound on the activation of thymocytes. As shown in Figure 5C, treatment of mouse thymocytes with 15  $\mu\text{M}$  **8b** effectively caused an increase in the activation of double-positive (DP) thymocytes, as evidenced by increased surface expression of CD69, and increased expression of Nur77, an immediate early gene induced in thymocytes upon TCR stimulation (Figure 5D).<sup>47</sup> Taken together, these data indicate that **8b** is effective at inhibition of LYP/PEP in T cells, increasing both early TCR signaling and downstream T cell activation.

### Compound **8b** down-regulates mast cell action and inhibits anaphylaxis in mice

Anaphylaxis is controlled by rapid lipid mediator release, degranulation and by pro-inflammatory cytokine synthesis in mast cells.<sup>48</sup> Activated mast cells promote allergic inflammation following the release of biochemical mediators.<sup>49</sup> IgE mediated signaling through the LAT-PLC $\gamma$ -Ca<sup>2+</sup> pathway does not only end up in activation of the activity of the transcription factor NF-AT but also leads to degranulation. Degranulation occurs through the process of exocytosis whereby cargo proteins and other molecules are loaded into vesicles and shuttled to different subcellular locations for fusion events.<sup>50</sup> It results in the release of preformed mediators like  $\beta$ -hexosaminidase, serotonin, neural proteases and, histamine from the mast cell granules which causes an increase in vascular permeability, bronchoconstriction and inflammatory reaction in the mucosa.

PEP was recently shown to function as a positive regulator of mast cell action because bone marrow derived mast cells (BMMC) from PEP<sup>-/-</sup> mice displayed impaired PLC $\gamma$ 1 phosphorylation and Ca<sup>2+</sup> mobilization.<sup>51</sup> In addition, mice deficient in PEP are less susceptible to passive systemic anaphylaxis.<sup>51</sup> Additionally, it was demonstrated that a gold (I) compound C28<sup>32</sup> that inhibits the action of LYP could mimic the decreased PLC $\gamma$ 1 phosphorylation and susceptibility to systemic anaphylaxis of the PEP<sup>-/-</sup> BMMC and reduced anaphylaxis in mice.<sup>51</sup> Here we characterized compound **8b** in mast cells and the passive systemic anaphylaxis mouse model and compared its effects with those of C28. As intracellular Ca<sup>2+</sup> controls the expression of the transcription factor NF-AT, we compared the activity of this transcription factor in BMMC derived from both wild-type and PEP<sup>-/-</sup> mice. Upon transfection of a plasmid containing multimerized NF-AT binding sites driving the expression of a luciferase gene, a strong decrease in both the basal and antigen induced activity of this transcription factor was noticed in the PEP<sup>-/-</sup> BMMC compared to PEP<sup>+/+</sup> BMMC (Figure 6A). Treatment of the PEP<sup>+/+</sup> BMMC with the LYP inhibitors showed a dose dependent down-regulation of both the basal and the antigen-mediated increase in luciferase activity (Figure 6A). The effect of 5  $\mu$ M **8b** was superior to the same concentration of C28 and a higher concentration (20  $\mu$ M) of the former compound was even more efficacious. Concentrations over 5  $\mu$ M C28 were not used in this study as they were found to be toxic to the cells. No significant effect of the LYP inhibitors was observed on the residual NF-AT activity that could be measured in the PEP<sup>-/-</sup> BMMC indicating that they both function by inhibiting the action of PEP. As calcium mobilization plays an essential proximal role in intracellular events leading to mast cell degranulation, studies on antigen-stimulated degranulation were carried out. BMMC from PEP<sup>-/-</sup> mice showed a reduced release of  $\beta$ -hexosaminidase compared to PEP<sup>+/+</sup> BMMC (Figure 6B). As in the case of the analysis of NF-AT activity, both LYP inhibitors C28 and **8b** down-regulated this response with the latter compound showing superiority over C28 in its action (Figure 6B). Neither compounds affected residual degranulation in the PEP<sup>-/-</sup> BMMC.

Antigen-induced degranulation of mast cells leads to exaggerated allergic reaction in the form of anaphylaxis.<sup>52</sup> We have previously reported that PEP<sup>-/-</sup> mice are less susceptible to passive systemic anaphylaxis compared to PEP<sup>+/+</sup> mice which was in agreement with degranulation results obtained with PEP<sup>+/+</sup> and PEP<sup>-/-</sup> BMMC.<sup>51</sup> We have also shown that compound C28 when given to mice in a final concentration of 5  $\mu$ M mimicked the effect of the PEP knock-out. We therefore carried out passive systemic anaphylaxis (PSA) in both wild type and PEP knockout mice to determine whether compound **8b** would also inhibit the anaphylaxis response (Figure 7). PEP<sup>+/+</sup> mice treated with LYP inhibitor **8b** were less susceptible to PSA compared to the untreated groups. These results confirm that compound **8b** is a potent inhibitor of anaphylaxis and that its effect is mediated at least in part through the inhibition of the action of PEP. Together, the results show that **8b** is capable of down-regulating calcium mediated transcription and degranulation in mast cells and inhibiting anaphylaxis in mice.

## Discussion and Conclusions

Because of its strong association with autoimmunity, LYP is an attractive target for potential pharmacological intervention in the treatment of a broad spectrum of autoimmune diseases. Unfortunately, there have been no reports of a truly potent and selective LYP inhibitor that can be used in preclinical and clinical investigation. This study illustrates a structure-based focused library approach to quickly produce the high-affinity and LYP-selective inhibitor **8b**. Using the 6-hydroxy-benzofuran-5-carboxylic acid moiety to anchor the inhibitor to the LYP active site, the success of this approach relies on the introduction of secondary binding elements to enhance on-target potency and impart selectivity against the off-target phosphatases. Compound **8b** exhibits greater than 9-fold selectivity over a large and diverse

panel of PTPs (Table 5). Analysis of the LYP•**8b** structure indicates that the inhibitor interacts primarily with amino acid residues in the P-loop, the pTyr recognition loop, and the Q-loop. Although residues Phe28 and Lys32 are unique to LYP, many of the contact residues are conserved among all PTPs. How does **8b** achieve its specificity for LYP? To address this question, we compared the structural features of the LYP active site and its surrounding pockets with 9 different PTPs. Figure 8 shows that these PTPs display significant differences in surface electrostatic potential and topology around the active site. Indeed, the corresponding binding sites for the 2-position substituted phenyl group and the 3-chlorophenyl ring in various PTPs are not exactly the same. Sequence comparison also reveals that residues within a 5 Å radius of **8b** binding residues are highly variable (data not shown), which may account for the diverse surface properties in and around the PTP active site. These three dimensional structural differences in the binding sites likely dictate **8b** binding specificity. Thus, the crystal structure of the LYP-inhibitor complex reveals that **8b** not only interacts with LYP's active site but also targets peripheral binding pockets in the vicinity of the active site that are unique to LYP, providing further support of the notion that it is possible to obtain inhibitor potency and selectivity across the conserved PTP family. Importantly, we demonstrate that LYP inhibitor **8b** is highly efficacious in inhibiting LYP-mediated signaling in T cells, thymocytes, and bone marrow derived mast cells, as well as blocking systemic anaphylaxis in mice. Collectively, our results show that the 6-hydroxy-benzofuran-5-carboxylic acid pTyr mimetic can be converted into highly potent and selective PTP inhibitory agents with excellent *in vivo* efficacy. Compound **8b** could serve as a starting point for the discovery of clinically useful LYP inhibitors as novel anti-autoimmune agents.

## Experimental Section

### Materials

Polyethylene glycol (PEG3350) and buffers for crystallization were purchased from Hampton Research Co. *p*-Nitrophenyl phosphate (*p*NPP) was purchased from Fluka Co. Dithiothreitol (DTT) was provided by Fisher (Fair Lawn, NJ). The Ubi-Renilla-luciferase construct was generated by replacing the growth hormone cDNA in pUbiGH<sup>53</sup> by Renilla reniformis luciferase cDNA (Promega). 3X NF-AT luciferase construct was generously provided by Laurie Glimcher, Boston, USA.

### General procedures for chemistry

Melting points were measured in capillary tubes with Stuart SMP10 melting point apparatus and are uncorrected. <sup>1</sup>H NMR spectra were obtained on a Bruker 500 MHz NMR instrument. The chemical shifts were reported as δ ppm relative to TMS, using the residual solvent peak as the reference unless otherwise noted. The following abbreviations were used to express the multiplicities: s = singlet; d = doublet; t = triplet; q = quartet; m = multiplet; br = broad. High-performance liquid chromatography (HPLC) purification was carried out on a Waters Delta 600 equipped with a Sunfire Prep C18 OBD column (30 × 150 mm, 5 mM) with methanol-water (both containing 0.1% TFA) as the mobile phase (gradient: 30–100% methanol, flow 10 mL/min). Purity analyses were performed on an Agilent Technology 1200 Series consisting of a G1379B degasser, a G1312A Binary Pump, a G1367A wellplate autosampler, a G1314B variable wavelength detector and a G6130A Quadrupole mass spectrometer. The column used was a Kinetex XB-C18, 2.6 μm, 50 × 4.6 mm, run at a flow rate of 0.7 mL/min. A linear gradient was used for both the blank and the sample from 5% to 100% MeOH/water (0.1% TFA). The blank run was subtracted from the sample run. All the final compounds were obtained in a highly pure form (>95%). Resolution mass spectra were obtained on an Agilent Technologies 6130 Quadrupole LC/MS. Accurate mass spectrometric analysis was performed on an Agilent Technologies 6250



TOF spectrometer. All reactions were monitored by thin layer chromatography (TLC) carried out on Dynamic Adsorbents silica gel plates (0.25 mm thick, 60F254), visualized by using UV (254 nm). All compounds used for biological assays were purified by HPLC and are at least of 95% purity based on HPLC analytical results monitored with 254 nm wavelengths. All reagents and solvents were purchased from commercially available sources (FisherSci, Aldrich, Acros, Alfa Aesar, TCI).

### Synthesis of compounds 3a–e

The structures of compounds **3a–e** are listed in Table 1, and their syntheses from compound **12** are shown in Schemes 1. Compound **12** was obtained following an established procedure.<sup>39</sup> **13a–e**, which were prepared by Sonogashira coupling of compound **12** and an appropriate alkyne, were subjected to cyclization with I<sub>2</sub> to yield benzofuran **14a–e**. Then, coupling of **14a–e** with trimethylsilylacetylene provided the desired compounds **3a–e** with additional deprotection.

### General procedures for the preparation of 13a–e

Under a nitrogen atmosphere, a Schlenk reaction tube was charged with the appropriate alkyne substrate (2.4 mmol), compound **8** (2 mmol), Et<sub>3</sub>N (8 mmol), Pd(PPh<sub>3</sub>)<sub>2</sub>Cl<sub>2</sub> (0.06 mmol), CuI (0.12 mmol) and DMF (5mL). After the mixture was stirred at room temperature for 12 h, water was added. The aqueous phase was then extracted 3 times with ethyl acetate. The organic phase was washed with brine, dried over Na<sub>2</sub>SO<sub>4</sub>, filtered and concentrated. The crude residues were purified by flash column chromatography on silica gel to give the products **13a–e**.

#### 7-Methoxy-2,2-dimethyl-6-(naphthalen-1-ylethynyl)-4H-benzo[d][1,3]dioxin-4-one (13a)

Pale yellow solid: mp 143–145 °C. <sup>1</sup>H NMR (500 MHz, CDCl<sub>3</sub>) δ 8.50 (d, J = 8.2 Hz, 1H), 8.20 (s, 1H), 7.85 (dd, J = 11.4, 7.1 Hz, 2H), 7.76 (dd, J = 7.1, 1.0 Hz, 1H), 7.61 (m, 1H), 7.54 (m, 1H), 7.46 (dd, J = 8.2, 7.2 Hz, 1H), 6.49 (s, 1H), 3.97 (s, 3H), 1.75 (s, 6H). <sup>13</sup>C NMR (125M, CDCl<sub>3</sub>) δ 166.11, 160.20, 157.88, 134.55, 133.27, 133.17, 130.21, 128.80, 128.23, 126.81, 126.41, 126.32, 125.23, 120.81, 108.70, 106.73, 99.05, 91.69, 88.71, 56.50, 25.85. Mass spectra (ESI): m/e 359 (M + H)<sup>+</sup>. HRMS (ESI) calcd for C<sub>23</sub>H<sub>19</sub>O<sub>4</sub><sup>+</sup> [(M + H)<sup>+</sup>], 359.1278; found, 359.1268.

#### 6-([1,1'-Biphenyl]-4-ylethynyl)-7-methoxy-2,2-dimethyl-4H-benzo[d][1,3]dioxin-4-one (13b)

Orange solid: mp 175–176 °C. <sup>1</sup>H NMR (500 MHz, CDCl<sub>3</sub>) δ 8.11 (s, 1H), 7.61 (br, 6H), 7.36 (m, 1H), 6.45 (s, 1H), 3.95 (s, 3H), 1.75 (s, 6H). <sup>13</sup>C NMR (125M, CDCl<sub>3</sub>) δ 165.98, 160.14, 157.83, 141.03, 140.33, 135.21, 134.78, 132.95, 132.05, 128.91, 127.87, 127.64, 126.98, 108.50, 106.72, 99.01, 93.28, 84.42, 56.46, 25.86. Mass spectra (ESI): m/e 385 (M + H)<sup>+</sup>. HRMS (ESI) calcd for C<sub>25</sub>H<sub>21</sub>O<sub>4</sub><sup>+</sup> [(M + H)<sup>+</sup>], 385.1434; found, 359.1441.

#### 6-((3-Chlorophenyl)ethynyl)-7-methoxy-2,2-dimethyl-4H-benzo[d][1,3]dioxin-4-one (13c)

Yellow solid: mp 138–139. <sup>1</sup>H NMR (500 MHz, CDCl<sub>3</sub>) δ 8.08 (s, 1H), 7.52 (t, J = 1.4 Hz, 1H), 7.40 (m, 1H), 7.29 (m, 2H), 6.45 (s, 1H), 3.95 (s, 3H), 1.75 (s, 6H). <sup>13</sup>C NMR (125M, CDCl<sub>3</sub>) δ 166.18, 160.15, 158.19, 135.01, 134.25, 131.53, 129.86, 129.67, 128.67, 125.00, 108.05, 106.88, 106.13, 99.18, 91.93, 85.10, 56.60, 25.98. Mass spectra (ESI): m/e 343 (M + H)<sup>+</sup>. HRMS (ESI) calcd for C<sub>19</sub>H<sub>16</sub>ClO<sub>4</sub><sup>+</sup> [(M + H)<sup>+</sup>], 343.0732; found, 343.0730.

**7-Methoxy-2,2-dimethyl-6-((4-(trifluoromethoxy)phenyl)ethynyl)-4H-benzo[d][1,3]dioxin-4-one (13d)**

Pale yellow solid: mp 128–130 °C. <sup>1</sup>H NMR (500 MHz, CDCl<sub>3</sub>) δ 8.09 (s, 1H), 7.55 (dt, J = 8.6, 2.0 Hz, 2H), 7.19 (d, J = 8.6 Hz, 2H), 6.45 (s, 1H), 3.95 (s, 3H), 1.75 (s, 6H). <sup>13</sup>C NMR (125M, CDCl<sub>3</sub>) δ 166.15, 160.21, 158.16, 149.06, 135.02, 133.26, 122.10, 120.99, 108.16, 106.91, 106.16, 99.19, 91.94, 84.73, 56.61, 25.99. Mass spectra (ESI): m/e 393 (M + H)<sup>+</sup>. HRMS (ESI) calcd for C<sub>20</sub>H<sub>16</sub>F<sub>3</sub>O<sub>5</sub><sup>+</sup> [(M + H)<sup>+</sup>], 393.0944; found, 393.0938.

**7-Methoxy-2,2-dimethyl-6-((4-phenoxyphenyl)ethynyl)-4H-benzo[d][1,3]dioxin-4-one (13e)**

White solid: mp 138–140 °C. <sup>1</sup>H NMR (500 MHz, CDCl<sub>3</sub>) δ 8.07 (s, 1H), 7.49 (dt, J = 8.8, 2.0 Hz, 2H), 7.36 (m, 2H), 7.14 (tt, J = 7.4, 1.0 Hz, 1H), 7.04 (m, 2H), 6.96 (dt, J = 8.8, 2.0 Hz, 2H), 6.44 (s, 1H), 3.94 (s, 3H), 1.75 (s, 6H). Mass spectra (ESI): m/e 401 (M + H)<sup>+</sup>. HRMS (ESI) calcd for C<sub>25</sub>H<sub>21</sub>O<sub>5</sub><sup>+</sup> [(M + H)<sup>+</sup>], 401.1384; found, 401.1394.

**General procedures for the preparation of 15a–e**

Compounds **15a–e** were synthesized in two steps from compounds **13a–e**. Compounds **14a–e** were prepared from compounds **13a–e** using procedures similar to those described in the literature.<sup>39</sup> To a solution of compounds **13a–e** in acetonitrile, two equivalents of iodine and NaHCO<sub>3</sub> were added. After stirring at 70 °C for 12 h, one additional equivalent of iodine and NaHCO<sub>3</sub> were added and the resulting mixtures were heated for another 12 h. Then the solvent was removed and ethyl acetate was added. The organic phase was washed with saturated aqueous Na<sub>2</sub>SO<sub>3</sub>, H<sub>2</sub>O, and saturated aqueous NaCl, and dried over Na<sub>2</sub>SO<sub>4</sub>. Solvent was removed by evaporation to leave the iodide as yellow solids which were used in the next step without further purification. The crude iodide **14a–e** were reacted with trimethylsilylacetylene in the presence of catalytic amounts of Pd(PPh<sub>3</sub>)<sub>2</sub>Cl<sub>2</sub> and CuI to give compounds **15a–e**.

**2,2-Dimethyl-7-(naphthalen-1-yl)-6-((trimethylsilyl)ethynyl)-4H-[1,3]dioxino[5,4-f]benzofuran-4-one (15a)**

White solid: mp 181–182 °C. <sup>1</sup>H NMR (500 MHz, CDCl<sub>3</sub>) δ 8.41 (s, 1H), 8.26 (m, 1H), 8.05 (d, J = 7.0 Hz, 1H), 7.98 (d, J = 8.2 Hz, 1H), 7.92 (m, 1H), 7.57 (m, 3H), 7.14 (s, 1H), 1.77 (s, 6H), 0.18 (s, 9H). Mass spectra (ESI): m/e 441 (M + H)<sup>+</sup>. HRMS (ESI) calcd for C<sub>27</sub>H<sub>25</sub>O<sub>4</sub>Si<sup>+</sup> [(M + H)<sup>+</sup>], 441.1517; found, 441.1516.

**7-([1,1'-Biphenyl]-4-yl)-2,2-dimethyl-6-((trimethylsilyl)ethynyl)-4H-[1,3]dioxino[5,4-f]benzofuran-4-one (15b)**

Pale yellow solid: mp 185–186 °C. <sup>1</sup>H NMR (500 MHz, CDCl<sub>3</sub>) δ 8.34 (s, 1H), 8.32 (s, 2H), 7.70 (m, 2H), 7.66 (m, 2H), 7.47 (t, J = 7.9 Hz, 2H), 7.40 (m, 1H), 7.06 (s, 1H), 1.76 (s, 6H), 0.36 (s, 9H). <sup>13</sup>C NMR (125M, CDCl<sub>3</sub>) δ 161.51, 158.35, 157.71, 154.59, 142.43, 140.27, 129.05, 128.27, 127.99, 127.37, 127.18, 126.44, 126.01, 122.55, 110.67, 106.63, 104.77, 99.97, 99.48, 95.50, 25.98, 0.13. Mass spectra (ESI): m/e 467 (M + H)<sup>+</sup>. HRMS (ESI) calcd for C<sub>29</sub>H<sub>27</sub>O<sub>4</sub>Si<sup>+</sup> [(M + H)<sup>+</sup>], 467.1673; found, 467.1679.

**7-(3-Chlorophenyl)-2,2-dimethyl-6-((trimethylsilyl)ethynyl)-4H-[1,3]dioxino[5,4-f]benzofuran-4-one(15c)**

White solid: mp 208–209 °C. <sup>1</sup>H NMR (500 MHz, CDCl<sub>3</sub>) δ 8.36 (t, J = 1.7 Hz, 1H), 8.08 (dt, J = 7.5, 1.6 Hz, 1H), 7.39 (m, 2H), 7.07 (s, 1H), 1.77 (s, 6H), 0.35 (s, 9H). Mass spectra (ESI): m/e 425 (M + H)<sup>+</sup>. HRMS (ESI) calcd for C<sub>23</sub>H<sub>22</sub>ClO<sub>4</sub>Si<sup>+</sup> [(M + H)<sup>+</sup>], 425.0970; found, 425.0975.

### 2,2-Dimethyl-7-(4-(trifluoromethoxy)phenyl)-6-((trimethylsilyl)ethynyl)-4H-[1,3]dioxino[5,4-f]benzofuran-4-one (15d)

Pale yellow solid: mp 146–148 °C.  $^1\text{H}$  NMR (500 MHz,  $\text{CDCl}_3$ )  $\delta$  8.32 (s, 1H), 8.29 (m, 2H), 7.31 (d,  $J = 8.1$  Hz, 2H), 7.06 (s, 1H), 1.77 (s, 6H), 0.35 (s, 9H).  $^{13}\text{C}$  NMR (125M,  $\text{CDCl}_3$ )  $\delta$  161.38, 157.64, 156.96, 154.76, 149.91, 149.90, 128.02, 127.53, 125.71, 122.79, 121.08, 120.55 (q,  $J_{\text{CF}} = 256.5$  Hz), 110.86, 106.67, 105.17, 100.09, 95.00, 25.97, 0.03. Mass spectra (ESI):  $m/e$  475 ( $\text{M} + \text{H}$ ) $^+$ . HRMS (ESI) calcd for  $\text{C}_{24}\text{H}_{22}\text{F}_3\text{O}_5\text{Si}^+$  [( $\text{M} + \text{H}$ ) $^+$ ], 475.1183; found, 475.1187.

### 2,2-Dimethyl-7-(4-phenoxyphenyl)-6-((trimethylsilyl)ethynyl)-4H-[1,3]dioxino[5,4-f]benzofuran-4-one (15e)

Off-white solid: mp 175–177 °C.  $^1\text{H}$  NMR (500 MHz,  $\text{CDCl}_3$ )  $\delta$  8.30 (s, 1H), 8.23 (m, 2H), 7.71 (m, 1H), 7.53 (m, 1H), 7.39 (m, 2H), 7.18 (m, 1H), 7.09 (m, 5H), 7.05 (s, 1H), 1.76 (s, 6H), 0.35 (s, 9H). Mass spectra (ESI):  $m/e$  483 ( $\text{M} + \text{H}$ ) $^+$ . HRMS (ESI) calcd for  $\text{C}_{29}\text{H}_{27}\text{O}_5\text{Si}^+$  [( $\text{M} + \text{H}$ ) $^+$ ], 483.1622; found, 483.1600.

### General procedures for the preparation of 3a–e

To a solution of **15a–e** (0.2 mmol) in THF (2 mL), KOH (0.8 mmol) was added. The obtained mixtures were refluxed for 2 hours, then acidified with 3 M HCl and extracted with ethyl acetate. The organic layers were dried over anhydrous  $\text{Na}_2\text{SO}_4$ , filtered, and concentrated under reduced pressure. The residues were purified by HPLC to furnish the corresponding products **3a–e**.

### 3-Ethynyl-6-hydroxy-2-(naphthalen-1-yl)benzofuran-5-carboxylic Acid (3a)

Pale yellow solid: mp 213 °C (decomposition).  $^1\text{H}$  NMR (500 MHz,  $\text{DMSO}-d_6$ )  $\delta$  8.15 (m, 2H), 8.13 (s, 1H), 7.99 (d,  $J = 6.9$  Hz, 1H), 7.70 (t,  $J = 7.7$  Hz, 1H), 7.65 (m, 2H), 7.34 (s, 1H), 4.56 (s, 1H).  $^{13}\text{C}$  NMR (125M,  $\text{DMSO}-d_6$ )  $\delta$  171.95, 160.40, 158.46, 157.48, 133.36, 130.86, 130.00, 128.87, 128.61, 127.24, 126.56, 125.56, 125.39, 125.29, 121.75, 121.02, 110.15, 99.41, 87.84, 73.69. Mass spectra (ESI):  $m/e$  329 ( $\text{M} + \text{H}$ ) $^+$ . HRMS (ESI) calcd for  $\text{C}_{21}\text{H}_{11}\text{O}_4^-$  [( $\text{M} - \text{H}$ ) $^-$ ], 327.0663; found, 327.0659.

### 2-([1,1'-Biphenyl]-4-yl)-3-ethynyl-6-hydroxybenzofuran-5-carboxylic Acid (3b)

Yellow solid: mp 190 °C (decomposition).  $^1\text{H}$  NMR (500 MHz,  $\text{DMSO}-d_6$ )  $\delta$  8.25 (d,  $J = 8.5$  Hz, 2H), 8.04 (s, 1H), 7.90 (d,  $J = 8.5$  Hz, 2H), 7.77 (d,  $J = 7.5$  Hz, 2H), 7.51 (t,  $J = 7.5$  Hz, 2H), 7.42 (t,  $J = 7.5$  Hz, 1H), 7.27 (s, 1H), 4.98 (s, 1H).  $^{13}\text{C}$  NMR (125M,  $\text{DMSO}-d_6$ )  $\delta$  171.88, 160.56, 156.87, 156.47, 141.19, 138.95, 129.05, 128.05, 127.52, 127.24, 126.66, 125.69, 121.75, 121.57, 110.60, 99.49, 99.21, 97.69, 90.00, 74.28. Mass spectra (ESI):  $m/e$  355 ( $\text{M} + \text{H}$ ) $^+$ . HRMS (ESI) calcd for  $\text{C}_{23}\text{H}_{13}\text{O}_4^-$  [( $\text{M} - \text{H}$ ) $^-$ ], 353.0819; found, 353.0811.

### 2-(3-Chlorophenyl)-3-ethynyl-6-hydroxybenzofuran-5-carboxylic Acid (3c)

Pale yellow solid: mp 207 °C (decomposition).  $^1\text{H}$  NMR (500 MHz,  $\text{DMSO}-d_6$ )  $\delta$  8.05 (m, 2H), 7.95 (s, 1H), 7.55 (t,  $J = 7.9$  Hz, 1H), 7.50 (m, 1H), 7.16 (s, 1H), 4.97 (s, 1H).  $^{13}\text{C}$  NMR (125M,  $\text{DMSO}-d_6$ )  $\delta$  171.81, 160.75, 156.77, 154.72, 133.77, 130.98, 130.38, 129.40, 124.37, 123.53, 121.85, 121.37, 110.75, 99.14, 98.86, 90.50, 73.81. Mass spectra (ESI):  $m/e$  313 ( $\text{M} + \text{H}$ ) $^+$ . HRMS (ESI) calcd for  $\text{C}_{17}\text{H}_8\text{ClO}_4^-$  [( $\text{M} - \text{H}$ ) $^-$ ], 311.0117; found, 311.0113.

### 3-Ethynyl-6-hydroxy-2-(4-(trifluoromethoxy)phenyl)benzofuran-5-carboxylic Acid (3d)

Pale yellow solid: mp 185 °C (decomposition).  $^1\text{H}$  NMR (500 MHz,  $\text{DMSO}-d_6$ )  $\delta$  8.17 (d,  $J = 8.1$  Hz, 2H), 7.95 (s, 1H), 7.50 (d,  $J = 8.1$  Hz, 2H), 7.50 (d,  $J = 8.1$  Hz, 2H), 7.15 (s, 1H), 4.91 (s, 1H).  $^{13}\text{C}$  NMR (125M,  $\text{DMSO}-d_6$ )  $\delta$  160.72, 156.78, 155.12, 148.73, 127.65,

127.05, 121.77, 121.42, 119.99 (q,  $J_{CF} = 255.6$  Hz), 99.09, 98.41, 89.99, 73.85. Mass spectra (ESI):  $m/e$  363 (M + H)<sup>+</sup>. HRMS (ESI) calcd for C<sub>18</sub>H<sub>8</sub>F<sub>3</sub>O<sub>5</sub><sup>-</sup> [(M - H)<sup>-</sup>], 361.0329; found, 361.0333.

### 3-Ethynyl-6-hydroxy-2-(4-phenoxyphenyl)benzofuran-5-carboxylic Acid (3e)

Pale yellow solid: mp 182 °C (decomposition). <sup>1</sup>H NMR (500 MHz, DMSO-*d*<sub>6</sub>) δ 8.14 (d, J = 8.8 Hz, 2H), 7.98 (s, 1H), 7.45 (t, J = 7.9 Hz, 2H), 7.22 (m, 2H), 7.13 (m, 4H), 4.86 (s, 1H). <sup>13</sup>C NMR (125M, DMSO-*d*<sub>6</sub>) δ 171.87, 160.42, 158.17, 156.70, 156.49, 155.53, 130.23, 127.23, 124.30, 123.50, 121.72, 121.36, 119.47, 118.37, 99.49, 99.10, 96.63, 89.38, 74.27. Mass spectra (ESI):  $m/e$  371 (M + H)<sup>+</sup>. HRMS (ESI) calcd for C<sub>23</sub>H<sub>13</sub>O<sub>5</sub><sup>-</sup> [(M - H)<sup>-</sup>], 369.0768; found, 369.0771.

### Synthesis of compounds 4a–i

3-substituted analogues **4a–i**, listed in Table 2, were synthesized according to established procedures,<sup>39</sup> shown in Scheme 2.

### Synthesis of compounds 5a–d

The structures of compounds **5a–d** are listed in Table 3, and their syntheses from compound **14d** are shown in Schemes 3.

### General procedures for the preparation of 19a–d

Under a nitrogen atmosphere, a Schlenk reaction tube was charged with appropriate alkyne substrate (2.4 mmol), compound **14d** (2 mmol), Et<sub>3</sub>N (8 mmol), Pd(PPh<sub>3</sub>)<sub>2</sub>Cl<sub>2</sub> (0.06 mmol), CuI (0.12 mmol) and DMF (5mL). After the mixture was heated (45 °C) overnight, water was added. The aqueous phase was then extracted 3 times with ethyl acetate. The organic phase was washed with brine, dried over Na<sub>2</sub>SO<sub>4</sub>, filtered and concentrated. The crude residues were purified by flash column chromatography on silica gel to give the products **19a–d**.

### 6-((3-Chlorophenyl)ethynyl)-2,2-dimethyl-7-(4-(trifluoromethoxy)phenyl)-4H-[1,3]dioxino[5,4-f]benzofuran-4-one (19a)

White solid: mp 138–140 °C. <sup>1</sup>H NMR (500MHz, CDCl<sub>3</sub>) δ 8.36 (s, 1H), 8.28 (m, 2H), 7.59 (t, J = 1.7 Hz, 1H), 7.49 (dt, J = 7.3, 1.4 Hz, 1H), 7.37 (m, 4H), 7.10 (s, 1H), 1.75 (s, 6H). <sup>13</sup>C NMR (125M, CDCl<sub>3</sub>) δ 161.20, 157.69, 156.31, 154.74, 149.89, 134.51, 131.38, 129.86, 129.79, 129.29, 127.81, 127.47, 125.52, 124.16, 122.53, 121.17, 120.43 (q, JCF = 256.8 Hz), 110.84, 106.64, 100.04, 99.99, 96.67, 80.57, 25.88. Mass spectra (ESI):  $m/e$  513 (M + H)<sup>+</sup>. HRMS (ESI) calcd for C<sub>27</sub>H<sub>17</sub>ClF<sub>3</sub>O<sub>5</sub><sup>+</sup> [(M + H)<sup>+</sup>], 513.0711; found, 513.0708.

### 6-((3,4-Dichlorophenyl)ethynyl)-2,2-dimethyl-7-(4-(trifluoromethoxy)phenyl)-4H-[1,3]dioxino[5,4-f]benzofuran-4-one (19b)

Off-white solid: mp 158–160 °C. <sup>1</sup>H NMR (500MHz, CDCl<sub>3</sub>) δ 8.34 (s, 1H), 8.26 (m, 2H), 7.68 (d, J = 1.9 Hz, 1H), 7.49 (d, J = 8.3 Hz, 1H), 7.42 (dd, J = 8.3, 1.9 Hz, 1H), 7.36 (d, J = 8.3 Hz, 2H), 7.10 (s, 1H), 1.77 (s, 6H). <sup>13</sup>C NMR (125M, CDCl<sub>3</sub>) δ 161.18, 151.68, 156.47, 154.78, 149.97, 149.96, 133.54, 133.08, 132.97, 130.71, 130.69, 127.71, 127.48, 125.39, 122.47, 122.38, 121.18, 120.43 (q, JCF = 256.3 Hz), 110.88, 106.67, 100.09, 100.00, 99.28, 95.70, 81.40, 25.88. Mass spectra (ESI):  $m/e$  547 (M + H)<sup>+</sup>. HRMS (ESI) calcd for C<sub>27</sub>H<sub>16</sub>Cl<sub>2</sub>F<sub>3</sub>O<sub>5</sub><sup>+</sup> [(M + H)<sup>+</sup>], 547.0321; found, 513.0333.

**2,2-Dimethyl-6-(thiophen-3-ylethynyl)-7-(4-(trifluoromethoxy)phenyl)-4H-[1,3]dioxino[5,4-f]benzofuran-4-one (19c)**

Off-white solid: mp 160–162 °C. <sup>1</sup>H NMR (500MHz, CDCl<sub>3</sub>) δ 8.37 (s, 1H), 8.29 (m, 2H), 7.64 (dd, J = 3.0, 1.2 Hz, 1H), 7.38 (dd, J = 5.0, 3.0 Hz, 1H), 7.33 (m, 2H), 7.28 (dd, J = 5.0, 1.2 Hz, 1H), 7.08 (s, 1H), 1.77 (s, 6H). <sup>13</sup>C NMR (125M, CDCl<sub>3</sub>) δ 161.41, 157.80, 155.94, 154.78, 149.84, 149.83, 129.85, 129.71, 128.07, 127.45, 126.03, 125.82, 122.73, 121.66, 121.22, 120.55 (q, JCF = 256.44 Hz), 110.83, 106.72, 100.08, 100.05, 93.57, 25.99. Mass spectra (ESI): m/e 585 (M + H)<sup>+</sup>. HRMS (ESI) calcd for C<sub>25</sub>H<sub>16</sub>F<sub>3</sub>O<sub>5</sub>S<sup>+</sup> [(M + H)<sup>+</sup>], 485.0665; found, 485.0666.

**Methyl 2-(3-((2,2-dimethyl-4-oxo-7-(4-(trifluoromethoxy)phenyl)-4H-[1,3]dioxino[5,4-f]benzofuran-6-yl)ethynyl)phenoxy)acetate (19d)**

Off-White solid: mp 118–119 °C. <sup>1</sup>H NMR (500MHz, CDCl<sub>3</sub>) δ 8.37 (s, 1H), 8.30 (m, 2H), 7.35 (m, 3H), 7.27 (m, 1H), 7.14 (m, 1H), 7.09 (s, 1H), 6.99 (dd, J = 8.4, 2.7 Hz, 1H), 4.71 (s, 2H), 3.85 (s, 3H), 1.78 (s, 6H). <sup>13</sup>C NMR (125M, CDCl<sub>3</sub>) δ 169.22, 161.39, 157.85, 157.83, 156.26, 154.81, 130.01, 128.02, 127.55, 125.73, 125.46, 123.85, 122.71, 121.26, 120.55 (q, JCF = 256.44 Hz), 117.46, 116.15, 110.88, 106.74, 100.13, 99.91, 97.90, 79.69, 65.48, 52.51, 25.99. Mass spectra (ESI): m/e 567 (M + H)<sup>+</sup>. HRMS (ESI) calcd for C<sub>30</sub>H<sub>22</sub>F<sub>3</sub>O<sub>8</sub><sup>+</sup> [(M + H)<sup>+</sup>], 567.1261; found, 567.1241.

**General procedure for the preparation of 5a–d**

To a solution of **19a–d** (0.2 mmol) in MeOH (2 mL), KOH (0.8 mmol) was added. The obtained mixtures were refluxed for 2 hours, then acidified with 3 M HCl and extracted with ethyl acetate. The organic layers were dried over anhydrous Na<sub>2</sub>SO<sub>4</sub>, filtered, and concentrated under reduced pressure. The residues were purified by HPLC to furnish the corresponding products **5a–d**.

**3-((3-Chlorophenyl)ethynyl)-6-hydroxy-2-(4-(trifluoromethoxy)phenyl)benzofuran-5-carboxylic Acid (5a)**

Off-white solid: mp 196 °C (decomposition). <sup>1</sup>H NMR (500MHz, DMSO-*d*<sub>6</sub>) δ 8.23 (d, J = 8.8 Hz, 2H), 8.09 (s, 1H), 7.78 (br, 1H), 7.66 (d, J = 7.6 Hz, 1H), 7.56 (m, 3H), 7.50 (t, J = 7.8 Hz, 1H), 7.19 (s, 1H). <sup>13</sup>C NMR (125M, DMSO-*d*<sub>6</sub>) δ 171.83, 160.70, 156.87, 154.75, 148.72, 133.38, 130.73, 130.57, 130.25, 129.29, 127.61, 127.18, 123.60, 122.06, 121.49, 120.95, 119.94 (q, JCF = 252.9 Hz), 110.77, 99.45, 99.06, 98.63, 96.05, 80.67. Mass spectra (ESI): m/e 473 (M + H)<sup>+</sup>. HRMS (ESI) calcd for C<sub>24</sub>H<sub>11</sub>ClF<sub>3</sub>O<sub>5</sub><sup>-</sup> [(M - H)<sup>-</sup>], 471.0253; found, 471.0247.

**3-((3,4-Dichlorophenyl)ethynyl)-6-hydroxy-2-(4-(trifluoromethoxy)phenyl)benzofuran-5-carboxylic Acid (5b)**

Off-white solid: mp 213 °C (decomposition). <sup>1</sup>H NMR (500MHz, DMSO-*d*<sub>6</sub>) δ 8.33 (d, J = 8.7 Hz, 2H), 8.20 (s, 1H), 8.01 (s, 1H), 7.72 (br, 2H), 7.59 (d, J = 8.7 Hz, 2H), 7.20 (s, 1H). <sup>13</sup>C NMR (125M, DMSO-*d*<sub>6</sub>) δ 172.48, 161.49, 157.52, 155.28, 149.38, 133.25, 132.25, 132.66, 132.15, 131.95, 131.27, 128.18, 127.71, 122.84, 122.65, 121.86, 120.49 (q, JCF = 255.21 Hz), 99.99, 99.34, 99.07, 95.89, 81.97. Mass spectra (ESI): m/e 507 (M + H)<sup>+</sup>. HRMS (ESI) calcd for C<sub>24</sub>H<sub>10</sub>Cl<sub>2</sub>F<sub>3</sub>O<sub>5</sub><sup>-</sup> [(M - H)<sup>-</sup>], 504.9863; found, 504.9876.

**6-Hydroxy-3-(thiophen-3-ylethynyl)-2-(4-(trifluoromethoxy)phenyl)benzofuran-5-carboxylic Acid (5c)**

Off-white solid: mp 206 °C (decomposition). <sup>1</sup>H NMR (500MHz, DMSO-*d*<sub>6</sub>) δ 8.26 (m, 2H), 8.12 (m, 1H), 8.07 (s, 1H), 7.73 (dd, J = 5.0, 3.0 Hz, 1H), 7.57 (d, J = 8.4 Hz, 2H), 7.44

(dd,  $J = 5.0, 1.0$  Hz, 1H), 7.22 (s, 1H).  $^{13}\text{C}$  NMR (125M, DMSO- $d_6$ )  $\delta$  171.86, 160.65, 156.93, 154.27, 148.62, 130.93, 129.66, 127.80, 127.12, 126.99, 121.97, 121.49, 121.15, 120.57, 119.97 (q, JCF = 255.6 Hz), 110.60, 99.11, 93.28, 78.69. Mass spectra (ESI):  $m/e$  445 ( $M + H$ ) $^+$ . HRMS (ESI) calcd for  $\text{C}_{22}\text{H}_{10}\text{Cl}_2\text{F}_3\text{O}_5\text{S}^-$  [( $M - H$ ) $^-$ ], 443.0207; found, 443.0227.

### 3-((3-(Carboxymethoxy)phenyl)ethynyl)-6-hydroxy-2-(4-(trifluoromethoxy)phenyl)benzofuran-5-carboxylic Acid (5d)

Off-white solid: mp 190 °C (decomposition).  $^1\text{H}$  NMR (500MHz, DMSO- $d_6$ )  $\delta$  13.10 (br, 1H), 8.26 (m, 2H), 8.11 (s, 1H), 7.59 (d,  $J = 8.5$  Hz, 2H), 7.41 (t,  $J = 7.8$  Hz, 1H), 7.31 (d,  $J = 7.8$  Hz, 1H), 7.25 (m, 1H), 7.23 (s, 1H), 7.07 (dd,  $J = 8.5$  Hz, 2.4 Hz, 1H), 4.80 (s, 2H). Mass spectra (ESI):  $m/e$  513 ( $M + H$ ) $^+$ . HRMS (ESI) calcd for  $\text{C}_{26}\text{H}_{14}\text{F}_3\text{O}_8^-$  [( $M - H$ ) $^-$ ], 511.0646; found, 511.0643.

### Synthesis of compounds 6a and 6b

The structures and synthesis of compounds **6a** and **6b** are shown in Scheme 4.

### Methyl 2-(3-ethynylphenoxy)acetate (23) and methyl 2-(4-ethynylphenoxy)acetate (27)

Compounds **23** and **27** were synthesized from compounds **21** and **25** via Sonogashira coupling.<sup>54</sup> Compounds **21** and **25** were reacted with trimethylsilylacetylene in the presence of catalytic amounts of  $\text{Pd}(\text{PPh}_3)_2\text{Cl}_2$  and  $\text{CuI}$  to give compounds **22** and **26**, which were treated with TBAF to furnish compounds **23** and **27**. Compound **23**: White solid: mp 50–51 °C.  $^1\text{H}$  NMR (500MHz,  $\text{CDCl}_3$ )  $\delta$  7.23 (m, 1H), 7.13 (d,  $J = 7.6$  Hz, 1H), 7.01 (s, 1H), 6.92 (m, 1H), 4.62 (s, 2H), 3.80 (s, 3H), 3.08 (s, 1H).  $^{13}\text{C}$  NMR (125M,  $\text{CDCl}_3$ )  $\delta$  169.09, 157.49, 129.60, 125.76, 123.33, 117.81, 115.93, 83.22, 77.46, 65.23, 52.32. HRMS (ESI) calcd for  $\text{C}_{10}\text{H}_{11}\text{O}_3^+$  [( $M + H$ ) $^+$ ], 191.0703; found, 191.0716. Compound **27**: White solid: mp 82–83 °C.  $^1\text{H}$  NMR (500MHz,  $\text{CDCl}_3$ )  $\delta$  7.42 (dt,  $J = 8.9, 2.1$  Hz, 2H), 6.84 (dt,  $J = 8.9, 2.1$  Hz, 2H), 4.62 (s, 2H), 3.78 (s, 3H), 3.02 (s, 1H).  $^{13}\text{C}$  NMR (125M,  $\text{CDCl}_3$ )  $\delta$  169.00, 158.04, 133.70, 115.43, 114.62, 83.32, 76.36, 65.14, 52.34. HRMS (ESI) calcd for  $\text{C}_{10}\text{H}_{11}\text{O}_3^+$  [( $M + H$ ) $^+$ ], 191.0703; found, 191.0711.

### Methyl 2-(3-((7-methoxy-2,2-dimethyl-4-oxo-4H-benzo[d][1,3]dioxin-6-yl)ethynyl)phenoxy)acetate (28)

Under a nitrogen atmosphere, a Schlenk reaction tube was charged with compound **23** (12 mmol), compound **12** (10 mmol),  $\text{Et}_3\text{N}$  (40 mmol),  $\text{Pd}(\text{PPh}_3)_2\text{Cl}_2$  (0.3 mmol),  $\text{CuI}$  (0.6 mmol) and DMF (50 mL). After the mixture was stirred at room temperature overnight, water was added. The aqueous phase was then extracted 3 times with ethyl acetate. The organic phase was washed with brine, dried over  $\text{Na}_2\text{SO}_4$ , filtered and concentrated. The crude residues were purified by flash column chromatography on silica gel to give the products **28**. Yellow solid: mp 44–46 °C.  $^1\text{H}$  NMR (500MHz,  $\text{CDCl}_3$ )  $\delta$  8.07 (s, 1H), 7.27 (m, 1H), 7.17 (m, 1H), 7.05 (m, 1H), 6.91 (m, 1H), 6.45 (s, 1H), 4.67 (s, 2H), 3.94 (s, 3H), 3.82 (s, 3H), 1.74 (s, 6H).  $^{13}\text{C}$  NMR (125M,  $\text{CDCl}_3$ )  $\delta$  169.19, 166.07, 160.19, 157.96, 157.56, 134.80, 129.61, 125.34, 124.38, 117.18, 115.58, 108.23, 106.79, 105.95, 99.10, 92.92, 93.98, 65.28, 56.52, 52.35, 25.86. Mass spectra (ESI):  $m/e$  397 ( $M + H$ ) $^+$ . HRMS (ESI) calcd for  $\text{C}_{22}\text{H}_{21}\text{O}_7^+$  [( $M + H$ ) $^+$ ], 397.1282; found, 397.1277.

### Methyl 2-(3-(6-iodo-2,2-dimethyl-4-oxo-4H-[1,3]dioxino[5,4-f]benzofuran-7-yl)phenoxy)acetate (29)

To a solution of compound **28** (5 mmol) in acetonitrile were added iodine (10 mmol) and  $\text{NaHCO}_3$  (10 mmol). After stirring at 70 °C for 12 h, additional 5 mmol iodine and 5 mmol  $\text{NaHCO}_3$  were added and the resulting mixture was heated for another 12 h. Then the

solvent was removed and ethyl acetate was added. The organic phase was washed with saturated aqueous Na<sub>2</sub>SO<sub>3</sub>, H<sub>2</sub>O, and saturated aqueous NaCl, and dried over Na<sub>2</sub>SO<sub>4</sub>. The crude residues were purified by flash column chromatography on silica gel to give the product **29**. Pale yellow solid: mp 206–207 °C. <sup>1</sup>H NMR (500MHz, CDCl<sub>3</sub>) δ 8.12 (s, 1H), 7.80 (d, J = 8.0 Hz, 1H), 7.70 (t, J = 2.0 Hz, 1H), 7.43 (t, J = 8.0 Hz, 1H), 7.08 (s, 1H), 7.02 (dd, J = 8.0, 2.5 Hz, 1H), 4.74 (s, 2H), 3.84 (s, 3H), 1.77 (s, 6H). <sup>13</sup>C NMR (125M, CDCl<sub>3</sub>) δ 169.11, 161.18, 157.98, 157.83, 154.85, 153.84, 130.49, 129.96, 128.78, 124.08, 120.83, 116.32, 113.38, 110.75, 106.59, 99.81, 65.40, 61.10, 52.40, 25.86. Mass spectra (ESI): m/e 509 (M + H)<sup>+</sup>. HRMS (ESI) calcd for C<sub>21</sub>H<sub>18</sub>IO<sub>7</sub><sup>+</sup> [(M + H)<sup>+</sup>], 509.0092; found, 509.0084.

### Methyl 2-(3-(6-((3-chlorophenyl)ethynyl)-2,2-dimethyl-4-oxo-4H-[1,3]dioxino[5,4-f]benzofuran-7-yl)phenoxy)acetate (**30**)

Under a nitrogen atmosphere, a Schlenk reaction tube was charged with 1-chloro-3-ethynylbenzene (8.4 mmol), compound **29** (7 mmol), Et<sub>3</sub>N (28 mmol), Pd(PPh<sub>3</sub>)<sub>2</sub>Cl<sub>2</sub> (0.21 mmol), CuI (0.42 mmol) and DMF (30 mL). After the mixture was stirred at room temperature overnight, water was added. The aqueous phase was then extracted 3 times with ethyl acetate. The organic phase was washed with brine, dried over Na<sub>2</sub>SO<sub>4</sub>, filtered and concentrated. The crude residues were purified by flash column chromatography on silica gel to give the product **30**. Off-white solid: mp 164 °C (decomposition). <sup>1</sup>H NMR (500MHz, CDCl<sub>3</sub>) δ 8.33 (s, 1H), 7.82 (m, 1H), 7.60 (m, 1H), 7.51 (dt, J = 7.3, 1.5 Hz, 1H), 7.43 (t, J = 8.05 Hz, 1H), 7.37 (m, 2H), 7.08 (s, 1H), 7.00 (m, 1H), 4.72 (s, 1H), 3.80 (s, 3H), 1.77 (s, 6H). <sup>13</sup>C NMR (125M, CDCl<sub>3</sub>) δ 169.17, 161.43, 158.17, 157.78, 154.77, 134.58, 131.47, 130.66, 130.29, 129.96, 129.94, 125.77, 124.46, 122.55, 119.65, 116.54, 111.98, 110.84, 106.74, 100.15, 100.12, 99.49, 96.83, 81.08, 65.45, 52.54, 26.01. Mass spectra (ESI): m/e 517 (M + H)<sup>+</sup>. HRMS (ESI) calcd for C<sub>29</sub>H<sub>22</sub>ClO<sub>7</sub><sup>+</sup> [(M + H)<sup>+</sup>], 517.1049; found, 517.1040.

### 2-(3-(Carboxymethoxy)phenyl)-3-((3-chlorophenyl)ethynyl)-6-hydroxybenzofuran-5-carboxylic Acid (**6a**)

To a solution of **30** (0.2 mmol) in THF (2 mL), KOH (0.8 mmol) was added. The obtained mixture was refluxed 2 hours, then acidified with 3 M HCl and extracted with ethyl acetate. The organic layers were dried over anhydrous Na<sub>2</sub>SO<sub>4</sub>, filtered, and concentrated under reduced pressure. The residue was purified by HPLC to furnish the corresponding product **6a**. Pale yellow solid: mp 162 °C (decomposition). <sup>1</sup>H NMR (500 MHz, DMSO-*d*<sub>6</sub>) δ 11.7 (br, 1H), 8.10 (s, 1H), 7.77 (m, 2H), 7.67 (m, 1H), 7.64 (d, J = 7.6 Hz, 1H), 7.53 (t, J = 7.6 Hz, 1H), 7.49 (m, 2H), 7.22 (s, 1H), 7.05 (dd, J = 8.3, 2.3 Hz, 1H), 4.77 (s, 2H). <sup>13</sup>C NMR (125M, DMSO-*d*<sub>6</sub>) δ 172.43, 170.41, 161.11, 158.51, 157.37, 156.50, 133.96, 131.22, 131.16, 130.91, 130.63, 130.23, 129.78, 124.25, 122.49, 121.64, 118.74, 116.59, 111.64, 111.13, 99.64, 98.75, 96.55, 81.61, 65.03. Mass spectra (ESI): m/e 463 (M + H)<sup>+</sup>. HRMS (ESI) calcd for C<sub>25</sub>H<sub>14</sub>ClO<sub>7</sub><sup>-</sup> [(M - H)<sup>-</sup>], 461.0434; found, 461.0427.

### Methyl 2-(4-((7-methoxy-2,2-dimethyl-4-oxo-4H-benzo[d][1,3]dioxin-6-yl)ethynyl)phenoxy)acetate (**31**)

Under a nitrogen atmosphere, a Schlenk reaction tube was charged with **27** (12 mmol), compound **12** (10 mmol), Et<sub>3</sub>N (40 mmol), Pd(PPh<sub>3</sub>)<sub>2</sub>Cl<sub>2</sub> (0.3 mmol), CuI (0.6 mmol) and DMF (50 mL). After the mixture was stirred at room temperature overnight, water was added. The aqueous phase was then extracted three times with ethyl acetate. The organic phase was washed with brine, dried over Na<sub>2</sub>SO<sub>4</sub>, filtered and concentrated to yield compound **31** as white solid: mp 160–161 °C. <sup>1</sup>H NMR (500MHz, CDCl<sub>3</sub>) δ 8.03 (s, 1H), 7.45 (m, 2H), 6.86 (m, 2H), 6.41 (s, 1H), 4.63 (s, 2H), 3.91 (s, 2H), 3.19 (s, 3H), 1.72 (s, 6H). <sup>13</sup>C NMR (125M, CDCl<sub>3</sub>) δ 169.09, 165.96, 160.23, 157.84, 157.73, 134.60, 133.24, 116.56, 114.71, 108.66, 106.75, 105.98, 99.06, 93.02, 82.85, 65.27, 56.51, 52.39, 25.90.

Mass spectra (ESI):  $m/e$  397 (M + H)<sup>+</sup>. HRMS (ESI) calcd for C<sub>22</sub>H<sub>21</sub>O<sub>7</sub><sup>+</sup> [(M + H)<sup>+</sup>], 397.1282; found, 397.1260.

### Methyl 2-(4-(6-iodo-2,2-dimethyl-4-oxo-4H-[1,3]dioxino[5,4-f]benzofuran-7-yl)phenoxy)acetate (32)

Following the method described for compound **29**, the expected compound **32** was obtained. Off-white solid: mp 193 °C (decomposition). <sup>1</sup>H NMR (500MHz, CDCl<sub>3</sub>) δ 8.11 (m, 2H), 8.08 (s, 1H), 7.05 (s, 1H), 7.02 (m, 2H), 4.72 (s, 2H), 3.84 (s, 3H), 1.77 (s, 6H). <sup>13</sup>C NMR (125M, CDCl<sub>3</sub>) δ 168.96, 161.27, 158.72, 157.97, 154.58, 154.32, 128.99, 128.91, 123.63, 122.85, 114.71, 110.56, 106.53, 99.68, 65.19, 59.21, 52.42, 25.85. Mass spectra (ESI):  $m/e$  509 (M + H)<sup>+</sup>. HRMS (ESI) calcd for C<sub>21</sub>H<sub>18</sub>IO<sub>7</sub><sup>+</sup> [(M + H)<sup>+</sup>], 509.0092; found, 509.0097.

### Methyl 2-(4-(6-((3-chlorophenyl)ethynyl)-2,2-dimethyl-4-oxo-4H-[1,3]dioxino[5,4-f]benzofuran-7-yl)phenoxy)acetate (33)

Following the method described for compound **30**, the titled compound **33** was obtained. White solid: mp 173–174 °C. <sup>1</sup>H NMR (500MHz, CDCl<sub>3</sub>) δ 8.28 (s, 1H), 8.17 (m, 2H), 7.56 (m, 1H), 7.46 (m, 1H), 7.35 (m, 2H), 7.03 (m, 3H), 4.72 (s, 2H), 3.84 (s, 3H), 1.76 (s, 6H). <sup>13</sup>C NMR (125M, CDCl<sub>3</sub>) δ 169.03, 161.45, 158.95, 157.81, 157.60, 154.40, 134.46, 131.34, 129.88, 129.80, 127.76, 125.87, 124.61, 123.09, 122.00, 115.02, 110.57, 106.61, 99.95, 97.47, 96.00, 81.33, 65.25, 52.51, 25.93. Mass spectra (ESI):  $m/e$  517 (M + H)<sup>+</sup>. HRMS (ESI) calcd for C<sub>29</sub>H<sub>22</sub>ClO<sub>7</sub><sup>+</sup> [(M + H)<sup>+</sup>], 517.1049; found, 517.1044.

### 2-(4-(Carboxymethoxy)phenyl)-3-((3-chlorophenyl)ethynyl)-6-hydroxybenzofuran-5-carboxylic Acid (6b)

Following the method described for compound **6a**, the title compound **6b** was obtained. Pale yellow solid: mp 171 °C (decomposition). <sup>1</sup>H NMR (500 MHz, DMSO-*d*<sub>6</sub>) δ 13.14 (br, 1H), 11.73 (br, 1H), 8.14 (d, J = 8.4 Hz, 2H), 8.11 (s, 1H), 7.80 (s, 1H), 7.67 (d, J = 7.1 Hz, 1H), 7.52 (m, 2H), 7.24 (s, 1H), 7.17 (d, J = 8.4 Hz, 2H), 4.80 (s, 2H). <sup>13</sup>C NMR (125M, DMSO-*d*<sub>6</sub>) δ 17.033, 159.44, 157.27, 157.19, 133.92, 131.15, 130.65, 129.59, 127.56, 124.49, 122.16, 121.85, 115.71, 99.99, 99.68, 96.55, 95.73, 81.99, 64.97, 31.15. Mass spectra (ESI):  $m/e$  463 (M + H)<sup>+</sup>. HRMS (ESI) calcd for C<sub>25</sub>H<sub>14</sub>ClO<sub>7</sub><sup>-</sup> [(M - H)<sup>-</sup>], 461.0434; found, 461.0441.

### Preparation Libraries 7 and 8

The libraries were set up in 96-well plates. Compound **6a**, **6b**, amines (Figure 2), 2-(1H-benzotriazole-1-yl)-1, 1, 3, 3-tetramethylammonium hexafluorophosphate (HBTU), N-hydroxybenzotriazole (HOBt), and diisopropylethylamine (DIPEA) were dissolved as following: 0.25 M for **6a–b**, 0.5 M for amines, 0.5 M for HBTU and HOBt, and 1.25 M for DIPEA solutions in dry DMF in 96-deep-well plates. First, 40 μL of stock **6a** or **6b** solution (0.25 M) was added to each well of a 96-well plate (reaction plate) excluding the 12<sup>th</sup> column, which contained all other reagents (amines, HBTU, HOBt, DIPEA, DMF, DMSO) as background controls. Next, 20 μL of HBTU and HOBt were transferred to the reaction plates from the 0.5 M 96-deep-well plates. After 5 minutes, 20 μL of DIPEA and amines were transferred to the reaction plates from the master 96-deep-well plates. The reaction plates were sealed and shaken for 24 hours at room temperature. The products were detected by LC/MS. Finally, 130 μL of DMSO was added to the each well to yield the final product concentration of 40 mM, according to a 100% yield. Compounds in the reaction plates were screened at both 10 and 1 μM concentrations to detect inhibition against LYP. The top hits from the libraries were selected and re-synthesized in large scale and purified by HPLC, and their inhibition constants for LYP and selectivity against other PTPs were determined..



**3-((3-Chlorophenyl)ethynyl)-6-hydroxy-2-(3-(2-((4-isopropylphenyl)amino)-2-oxoethoxy)phenyl)benzofuran-5-carboxylic Acid (7a)**

Off-white solid: mp 236 °C (decomposition). <sup>1</sup>H NMR (500 MHz, DMSO-*d*<sub>6</sub>) δ 10.05 (s, 1H), 8.15 (s, 1H), 7.86 (d, J = 8.0 Hz, 1H), 7.81 (s, 1H), 7.67 (d, J = 7.7 Hz, 1H), 7.55 (m, 4H), 7.47 (t, J = 7.7 Hz, 1H), 7.23 (s, 1H), 7.19 (d, J = 8.2 Hz, 2H), 7.15 (dd, J = 8.2 Hz, 2.3 Hz, 1H), 4.79 (s, 2H), 2.85 (m, 1H), 1.18 (s, 6H). <sup>13</sup>C NMR (125M, DMSO-*d*<sub>6</sub>) δ 171.93, 166.01, 160.74, 158.17, 156.90, 156.03, 143.83, 136.05, 133.49, 130.82, 130.69, 130.51, 130.20, 129.82, 129.32, 126.40, 123.80, 122.08, 121.14, 119.93, 118.47, 116.07, 111.89, 110.92, 99.52, 99.14, 98.37, 96.08, 81.15, 67.27, 32.88, 23.93. Mass spectra (ESI): m/e 580 (M + H)<sup>+</sup>. HRMS (ESI) calcd for C<sub>34</sub>H<sub>25</sub>ClNO<sub>6</sub><sup>-</sup> [(M - H)<sup>-</sup>], 578.1376; found, 578.1365.

**3-((3-Chlorophenyl)ethynyl)-6-hydroxy-2-(4-(2-oxo-2-(propylamino)ethoxy)phenyl)benzofuran-5-carboxylic Acid (8a)**

White solid: mp 224 °C (decomposition). <sup>1</sup>H NMR (500 MHz, DMSO-*d*<sub>6</sub>) δ 8.15 (m, 3H), 8.11 (s, 1H), 7.79 (t, J = 1.6 Hz, 1H), 7.66 (dt, J = 7.4, 1.3 Hz, 1H), 7.55 (dt, J = 8.7, 1.4 Hz, 1H), 7.23 (s, 1H), 7.19 (d, J = 8.9 Hz, 2H), 4.58 (s, 2H), 3.11 (m, 2H), 1.46 (m, 2H), 0.84 (t, J = 7.4 Hz, 3H). <sup>13</sup>C NMR (125M, DMSO-*d*<sub>6</sub>) δ 172.48, 167.53, 160.86, 159.47, 157.31, 133.94, 131.17, 130.64, 129.64, 127.60, 124.48, 122.26, 122.06, 121.83, 116.00, 99.99, 99.62, 96.63, 95.74, 81.99, 67.48, 40.90, 22.81, 11.78. Mass spectra (ESI): m/e 504 (M + H)<sup>+</sup>. HRMS (ESI) calcd for C<sub>28</sub>H<sub>21</sub>ClNO<sub>6</sub><sup>-</sup> [(M - H)<sup>-</sup>], 502.1063; found, 502.1081.

**3-((3-Chlorophenyl)ethynyl)-2-(4-(2-(cyclopropylamino)-2-oxoethoxy)phenyl)-6-hydroxybenzofuran-5-carboxylic Acid (8b)**

White solid: mp 201 °C (decomposition). <sup>1</sup>H NMR (500 MHz, DMSO-*d*<sub>6</sub>) δ 8.19 (m, 1H), 8.14 (m, 3H), 7.80 (m, 1H), 7.67 (m, 1H), 7.53 (m, 2H), 7.25 (s, 1H), 7.18 (m, 2H), 4.55 (s, 2H), 2.71 (m, 1H), 0.65 (m, 2H), 0.50 (m, 2H). <sup>13</sup>C NMR (125M, DMSO-*d*<sub>6</sub>) δ 171.64, 168.36, 161.25, 158.85, 156.47, 133.48, 130.72, 130.67, 130.15, 129.11, 127.04, 126.97, 124.12, 122.03, 121.38, 115.48, 99.52, 98.58, 96.29, 95.06, 81.93, 66.93, 22.19, 5.18. Mass spectra (ESI): m/e 502 (M + H)<sup>+</sup>. HRMS (ESI) calcd for C<sub>28</sub>H<sub>19</sub>ClNO<sub>6</sub><sup>-</sup> [(M - H)<sup>-</sup>], 500.0906; found, 500.0911.

**3-((3-Chlorophenyl)ethynyl)-6-hydroxy-2-(4-(2-oxo-2-(phenylamino)ethoxy)phenyl)benzofuran-5-carboxylic Acid (8c)**

White solid: mp 178 °C (decomposition). <sup>1</sup>H NMR (500 MHz, DMSO-*d*<sub>6</sub>) δ 11.70 (br, 1H), 10.14 (s, 1H), 8.17 (d, J = 8.9 Hz, 2H), 8.12 (s, 1H), 7.80 (m, 1H), 7.66 (m, 3H), 7.52 (m, 2H), 7.34 (t, J = 7.7 Hz, 2H), 7.25 (m, 3H), 7.09 (t, J = 7.4 Hz, 1H), 4.83 (s, 2H). <sup>13</sup>C NMR (125M, DMSO-*d*<sub>6</sub>) δ 166.13, 160.39, 159.12, 156.85, 156.82, 138.36, 133.47, 130.74, 130.70, 130.20, 129.17, 128.75, 127.19, 124.00, 123.73, 121.82, 121.60, 121.39, 119.71, 115.52, 99.52, 99.17, 96.17, 95.31, 81.49, 67.09. Mass spectra (ESI): m/e 538 (M + H)<sup>+</sup>. HRMS (ESI) calcd for C<sub>31</sub>H<sub>19</sub>ClNO<sub>6</sub><sup>-</sup> [(M - H)<sup>-</sup>], 536.0906; found, 536.0898.

**2-(4-(2-((3s,5s,7s)-Adamantan-1-ylamino)-2-oxoethoxy)phenyl)-3-((3-chlorophenyl)ethynyl)-6-hydroxybenzofuran-5-carboxylic Acid (8d)**

Pale yellow solid: mp 166 °C (decomposition). <sup>1</sup>H NMR (500 MHz, DMSO-*d*<sub>6</sub>) δ 8.14 (m, 3H), 7.80 (s, 1H), 7.66 (d, J = 7.5 Hz, 1H), 7.55 (m, 1H), 7.51 (t, J = 7.7 Hz, 1H), 7.42 (s, 1H), 7.25 (s, 1H), 7.17 (d, J = 8.9 Hz, 2H), 4.51 (s, 2H), 2.02 (m, 4H), 1.97 (m, 6H), 1.62 (m, 6H). Mass spectra (ESI): m/e 596 (M + H)<sup>+</sup>. HRMS (ESI) calcd for C<sub>35</sub>H<sub>29</sub>ClNO<sub>6</sub><sup>-</sup> [(M - H)<sup>-</sup>], 594.1689; found, 594.1694.

**3-((3-Chlorophenyl)ethynyl)-2-(4-(2-(4-(3,4-dichlorophenyl)piperidin-1-yl)-2-oxoethoxy)phenyl)-6-hydroxybenzofuran-5-carboxylic Acid (8e)**

Pale yellow solid: mp 123–124 °C. <sup>1</sup>H NMR (500 MHz, DMSO-*d*<sub>6</sub>) δ 8.14 (m, 3H), 7.80 (m, 1H), 7.66 (m, 1H), 7.54 (m, 2H), 7.42 (d, J = 8.9 Hz, 1H), 7.25 (s, 1H), 7.19 (d, J = 6.5 Hz, 2H), 7.18 (s, 1H), 6.97 (m, 1H), 5.02 (s, 2H), 3.61 (m, 4H), 3.30 (m, 2H), 3.21 (m, 2H), 3.17 (m, 1H). Mass spectra (ESI): m/e 674 (M + H)<sup>+</sup>. HRMS (ESI) calcd for C<sub>36</sub>H<sub>25</sub>Cl<sub>3</sub>NO<sub>6</sub><sup>-</sup> [(M - H)<sup>-</sup>], 672.0753; found, 672.0684.

**3-((3-Chlorophenyl)ethynyl)-2-(4-(2-((3,4-dimethoxybenzyl)amino)-2-oxoethoxy)phenyl)-6-hydroxybenzofuran-5-carboxylic Acid (8f)**

Pale yellow solid: mp 185 °C (decomposition). <sup>1</sup>H NMR (500 MHz, DMSO-*d*<sub>6</sub>) δ 8.63 (t, J = 6.0 Hz, 1H), 8.16 (d J = 8.9 Hz, 2H), 8.12 (s, 1H), 7.80 (m, 1H), 7.66 (m, 1H), 7.54 (m, 2H), 7.24 (s, 1H), 7.21 (m, 2H), 6.86 (m, 2H), 6.78 (m, 1H), 4.67 (s, 2H), 4.29 (d, J = 6.0 Hz, 2H), 3.70 (s, 6H). Mass spectra (ESI): m/e 612 (M + H)<sup>+</sup>. HRMS (ESI) calcd for C<sub>34</sub>H<sub>25</sub>ClNO<sub>8</sub><sup>-</sup> [(M - H)<sup>-</sup>], 601.1274; found, 601.1275.

**3-((3-Chlorophenyl)ethynyl)-2-(4-(2-((3,4-dichlorobenzyl)amino)-2-oxoethoxy)phenyl)-6-hydroxybenzofuran-5-carboxylic Acid (8g)**

Off-white solid: mp 135–136 °C. <sup>1</sup>H NMR (500 MHz, DMSO-*d*<sub>6</sub>) δ 8.26 (t, J = 5.8 Hz, 1H), 8.14 (m, 4H), 7.80 (m, 1H), 7.67 (m, 1H), 7.53 (d, J = 1.0 HZ, 2H), 7.24 (s, 1H), 7.17 (m, 3H), 4.57 (s, 2H), 3.40 (q, J = 6.8 Hz, 2H), 2.88 (t, J = 6.8 Hz, 2H). Mass spectra (ESI): m/e 634 (M + H)<sup>+</sup>. HRMS (ESI) calcd for C<sub>33</sub>H<sub>21</sub>Cl<sub>3</sub>NO<sub>6</sub><sup>-</sup> [(M - H)<sup>-</sup>], 632.0440; found, 632.0406.

**Expression and purification of the LYP catalytic domain**

N-terminal (His)<sub>6</sub>-tagged LYP catalytic domain (residues 1–303) was subcloned into pET28a. For protein expression, the LYP expressing construct was transformed into *Escherichia coli* BL21-(DE3). Transformed cells were grown at 37 °C in Luria broth (LB) containing 100 µg/mL ampicillin for 4 h until the OD<sub>600</sub> reached 0.6, and then induced for growth overnight at room temperature with 0.4 mM IPTG. Cells were harvested by centrifugation (6000 rpm for 15 min at 4 °C), and the cell pellets from 1.5 L of LB medium were suspended in 30 mL of ice-cold lysis buffer consisting of 5 mM imidazole, 500 mM NaCl, 20 mM Tris-HCl (pH 7.9), 0.05 mg/mL trypsin inhibitor, and 0.1 mM PMSF. The suspensions were passed twice through a French Press at 1000 psi, and the cell lysates were centrifuged at 4 °C for 30 min at 15000 rpm. The supernatants were mixed with 2 mL of Ni-NTA Agarose (His\*Bind Resin) (Qiagen) at 4 °C for 1 h, and then the mixture was transferred to an empty column. The column was washed with 200 mL of binding buffer (5 mM imidazole, 500 mM NaCl, 20 mM Tris-HCl (pH 7.9)), followed by 20 mL of wash buffer (20 mM imidazole, 500 mM NaCl, 20 mM Tris-HCl (pH 7.9)), and then eluted with 20 mL of elution buffer (200 mM imidazole, 500 mM NaCl, 20 mM Tris-HCl (pH 7.9), 5 mM DTT). The elution was dialyzed for 6 h at 4 °C against 1 L buffer A (50 mM NaCl, 20 mM MES (pH 5.8), 1 mM EDTA), and then loaded onto a Mono S column equilibrated at 4 °C with buffer A. The column was washed with 10 mL of buffer A and then eluted with a 40 mL of linear gradient of 0 to 1 M NaCl in buffer A. The column fractions were analyzed by measuring the absorbance at 280 nm and by carrying out SDS-PAGE analysis. The fractions were combined, concentrated at 4 °C to 1 mL using an Amicon concentrator and then loaded onto a gel filtration column Superdex 75. The column was eluted with buffer A, and then the fractions which contained protein were combined and concentrated to 8 mg/ml and stored at –80 °C. The LYP preparation was shown to be homogeneous by SDS-PAGE analysis.

## Crystallization and data collection

For co-crystallization of LYP with compound **8b**, 100  $\mu$ l of 7 mg/ml LYP was mixed with 4  $\mu$ l stock of compound **8b** (20 mM in DMSO). Crystals were then grown by vapor diffusion in hanging drops at room temperature. Drops containing 1:1 volumes of protein in stock buffer and reservoir solutions were equilibrated against the reservoir solution A (0.2 M sodium formate pH 7.2, 20% PEG3350). The crystal was transferred into a reservoir solution B (0.2 M sodium formate pH 7.2, 30% PEG3350, 1 mM **8b**, 5% DMSO), soaked for 10 minutes, and flash-cooled in liquid nitrogen. X-ray data were collected at 100 K at SBC-CAT beamline 19-BM at the Advanced Photon Source (Argonne, IL) equipped with a mosaic CCD detector. The crystals belong to space group  $P2_12_12_1$  with the following unit cell parameters:  $a = 46.19 \text{ \AA}$ ,  $b = 93.64 \text{ \AA}$  and  $c = 153.50 \text{ \AA}$ . There are two protein monomers in the asymmetric unit. All data were processed with HKL3000,<sup>55</sup> and the statistics are provided in Table 6.

## Structural refinement of LYP•8b

The structure of LYP•**8b** was solved by molecular replacement using the program AMoRe.<sup>56</sup> The structure of the LYP catalytic domain (PDB entry code 2P6X),<sup>40</sup> without the solvent molecules and other small molecules, was used as a search model. The map revealed the density for the bound compound **8b** in the active site of LYP. The structure was refined to 2.30  $\text{\AA}$  resolution with the program CNS1.1,<sup>57</sup> first using simulated annealing at 2,500 K, and then alternating positional and individual temperature factor refinement cycles. The progress of the refinement was evaluated by the improvement in the quality of the electron density maps, and the reduced values of the conventional R factor ( $R = \frac{\sum_h ||F_o| - |F_c||}{\sum_h |F_o|}$ ), and the free R factor (4.2% of the reflections omitted from the refinement).<sup>58</sup> Electron density maps were inspected and the model was modified on an interactive graphics workstation with the program O.<sup>59</sup> Finally, water molecules were added gradually as the refinement progressed. They were assigned in the  $|F_o| - |F_c|$  difference Fourier maps with a  $3\sigma$  cutoff level for inclusion in the model. The statistics of refinements were also provided in Table 6. Molecular graphics were prepared by using Pymol ([www.pymol.sourceforge.net](http://www.pymol.sourceforge.net)).

## Data deposition

The coordinates for the structure of the LYP•**8b** complex (PDB ID 4J51) have been deposited in the Protein Data Bank.

## Enzyme kinetic assay

PTP activity was assayed using *p*-nitrophenyl phosphate (*p*NPP) as a substrate in 3,3-dimethylglutarate buffer (50 mM 3,3-dimethylglutarate, pH 7.0, 1 mM EDTA, 150 mM NaCl) at 25 °C. The assays were performed in 96-well plates. Normally, to determine the  $IC_{50}$  values for LYP, the reaction was initiated by the addition of enzyme (final concentration at 20 nM) to a reaction mixture (0.2 mL) containing 5.0 mM ( $K_m$  for the substrate against LYP) *p*NPP with serial dilutions. To determine the  $IC_{50}$  values for other PTPs, the assays were carried out under the same conditions used for LYP except that the concentration of the *p*NPP was set at the corresponding  $K_m$  value for each PTP. All PTPs used in the study were recombinant proteins prepared in-house. Concentration of compounds used to determine  $IC_{50}$  values ranged from 0.2- to 5-fold of the  $IC_{50}$  values. The reaction rate was measured using a SpectraMax Plus 384 Microplate Spectrophotometer (Molecular Devices). To determine the mode of inhibition, the reactions were initiated by the addition of LYP (final concentration at 5 nM) to the reaction mixtures (0.2 mL) containing various concentrations of *p*NPP and inhibitor **8b**. Data were fitted using SigmaPlot Enzyme Kinetics Module (Systat Software, Inc.).

## Cell culture

Jurkat T cells expressing the SV-40 large T Antigen (JTag)<sup>60</sup> were kept at logarithmic growth in RPMI 1640 medium (Mediatech, Manassas, VA) supplemented with 10% fetal bovine serum (Omega Scientific, Tarzana, CA), 2 mM glutamine, 1 mM sodium pyruvate, 10 mM HEPES pH 7.3, 2.5 mg/ml D-glucose, 100 units/ml of penicillin and 100 µg/ml streptomycin (Life Technologies, Carlsbad, CA). Murine bone marrow derived mast cells (BMMC) were obtained from 4–6 week culture of cells from bone marrow of PEP<sup>+/+</sup> and PEP<sup>-/-</sup> mice essentially as described.<sup>61</sup> The cells were cultured in IMDM supplemented with 10% heat-inactivated fetal calf serum (FBS), 2 mM L-glutamine, 1 mM pyruvate, 5 ng/ml IL-3 and 100 ng/ml stem cell factor (SCF). Cells were cultured at 37 °C in a CO<sub>2</sub> incubator.

## Phospho-flow cytometry

JTag cells were pretreated with 15 µM compound **8b** or DMSO for 30 minutes in RPMI 1640 at 37°C. Cells were then stimulated with supernatants of C305 hybridoma<sup>62</sup> for 2 min at 37°C. Cells were fixed immediately with BD Cytfix buffer, permeabilized using BD Phosflow Perm Buffer III and stained with AlexaFluor-conjugated anti-pZAP-70(Y319) antibody according to the manufacturer's protocols (BD Biosciences, San Jose, CA). Cell fluorescence was analyzed by FACS using a BD LSR II (BD Biosciences). Data was analyzed using FlowJo software (TreeStar, Ashland, OR).

## Thymocyte isolation

Nur77<sup>GFP</sup> reporter mice were kindly provided by K. Hogquist (University of Minnesota, MN).<sup>47</sup> To isolate mouse thymocytes, thymi were homogenized and passed through a 70 µm nylon strainer. Cells were washed in RPMI-1640, and red blood cells were depleted following treatment of the cell pellets with RBC lysis buffer according to the manufacturer's protocol (eBioscience, San Diego, CA). Thymocytes then were further washed in RPMI-1640, counted, and used for the experiments described above.

## T cell activation assays

CD69 expression on JTag cells was measured following incubation with 15 µM **8b** or DMSO for 4.5 hours in RPMI 1640 at 37°C. Cells were then stained with a FITC-conjugated anti-CD69 antibody (Biolegend, San Diego, CA). CD69 and Nur77 expression on CD4 and CD8 double-positive (DP) mouse thymocytes from Nur77<sup>GFP</sup> reporter mice was measured following incubation with 15 µM **8b** or DMSO for 4.5 hours in RPMI 1640 at 37°C. Cells were then stained with PE-conjugated-anti-CD69, APC-conjugated-anti-CD8, eFluor-450-conjugated anti-CD4 and PerCP-Cy5.5-conjugated-anti-TCRβ antibodies (Biolegend and eBioscience). Nur77 expression was assessed by fluorescence of GFP. Cell fluorescence was analyzed by FACS using a BD LSR II (BD Biosciences, San Jose, CA). Data were analyzed using FlowJo software (TreeStar, Ashland, OR).

## Animals

PEP<sup>+/-</sup> mice on a C57BL/6 background were generated by Hasegawa et al.,<sup>63</sup> and kindly provided by Genentech Inc., South San Francisco, CA, USA. The mice were subsequently bred in house on the same background and crossed to obtain wild type and knockout littermates for the study. Nur77<sup>GFP</sup> were generously obtained from K. Hogquist. The genotypes of the mice were established by tissue biopsies and subsequent PCR analysis as previously described.<sup>47,51</sup> All the animal experiments were performed according to European and German statutory regulations.

### Passive systemic anaphylaxis (PSA)

PSA was carried out essentially as described by Obiri et al.<sup>51</sup> In brief, 8–9 month old female mice (20–25g) were sensitized by intra-peritoneal (i.p.) injection with anti-DNP IgE (1 mg/kg) for 24 h. Compound **8b** (20  $\mu$ M) per mouse or vehicle (PBS) were administered by IP injection 1 h to the end of sensitization period. Anaphylaxis was initiated by intravenous (i.v.) injection of 200  $\mu$ l dinitrophenyl human serum albumin DNP-HSA (1 mg/ml PBS). Body temperature was measured with a Microlife VT 1831 Vet-Temp (Tiershop, Trier, Germany) every 5 min over a period of 60 min.

### Luciferase Reporter Gene Analysis

$8 \times 10^6$  BMMC cells were transfected with 4.5  $\mu$ g 3X NFAT-luciferase and 0.8  $\mu$ g of pUbi-Renilla Luc vectors by electroporation using the Nucleofector II (Amaxa) Program T-023. The cells were then plated in 2 ml culture medium (IMDM supplemented with 10% heat-inactivated FBS, 2 mM L-glutamine, 1 mM pyruvate, 5 ng/ml IL-3 and 100 ng/ml SCF) for 24 h to recover from the electroporation. The cells were then left unsensitized or sensitized with anti-DNP IgE for 18 h. They were then left untreated or activated with DNP-HSA for 8 h. Thereafter they were lysed in passive lysis buffer (Promega Mannheim, Germany) and the lysates were centrifuged at 10,000 rpm for 10 min at 4° C. Firefly and Renilla luciferase activity were then measured using Perkin Elmer luminescence counter 1420 (Victor light).

### Measurement of $\beta$ hexosaminidase

$5 \times 10^6$  cells/ml BMMC from PEP<sup>+/+</sup> and PEP<sup>-/-</sup> mice were sensitized with anti DNP-IgE for 16 h and treated with C-28 (5  $\mu$ M), **8b** (5  $\mu$ M) or **8b** (20  $\mu$ M) for 1 h at the end of IgE incubation. The cells were then activated with DNP-HAS (200 ng/ml) for various time points. Cells were harvested washed and re-suspended in 100  $\mu$ l of Tyrodes buffer (135 mM NaCl, 5 mM KCl, 1 mM MgCl<sub>2</sub>, 1 mM CaCl<sub>2</sub>, 5 mM Glucose, 20 mM HEPES, pH 7.4) at 37°C and b-hexosaminidase activity determined in an Ultra micro-plate reader ELx808IU (Bio-Tec-Instruments, Inc.) at a wavelength of 405 nm as previously described.<sup>64</sup> Percent degranulation was calculated as the released activity/total activity  $\times 100$ .

### Acknowledgments

This work was supported in part by the National Institutes of Health Grants RO1CA152194 to Z.-Y. Z., RO1AI070544 to N.B., and funds from the DFG (SPP 1394) to A. C. B. C. S.M.S. is supported by a Postdoctoral Fellowship from the Juvenile Diabetes Research Foundation. Compound screening was carried out in the Chemical Genomics Core Facility at Indiana University School of Medicine. We thank Jutta Stober, Rebecca Dittus, Selma Huber and Manuela Sauer for their excellent technical assistance.

### Abbreviations Used

<b>LYP</b>	lymphoid-specific tyrosine phosphatase
<b>PTK</b>	protein tyrosine kinase
<b>PTP</b>	protein tyrosine phosphatase
<b>TCR</b>	T cell receptor
<b>Lck</b>	lymphoid T cell tyrosine kinase
<b>ZAP-70</b>	$\zeta$ -chain-associated protein kinase 70
<b>Csk</b>	Src C-terminal kinase
<b>pNPP</b>	<i>p</i> -nitrophenyl phosphate

<b>SAR</b>	structure-activity relationship
<b>DMF</b>	dimethylformamide
<b>IC<sub>50</sub></b>	concentration at 50% inhibition
<b>JTA<sub>g</sub></b>	Jurkat T leukemia cells expressing SV-40 large T antigen
<b>PEP</b>	PEST-domain-enriched tyrosine phosphatase
<b>BMMC</b>	bone marrow derived mast cells
<b>PSA</b>	passive systemic anaphylaxis
<b>DMSO</b>	dimethylsulfoxide
<b>TFA</b>	trifluoroacetic acid
<b>HBTU</b>	O-(benzotriazol-1-yl)-N,N,N',N'-tetramethyluronium hexafluorophosphate
<b>HOBt</b>	hydroxybenzotriazole
<b>DIPEA</b>	diisopropylethylamine
<b>THF</b>	tetrahydrofuran
<b>PBS</b>	phosphate-buffered saline
<b>FBS</b>	fetal bovine serum

## References

- Hunter T. Tyrosine phosphorylation: thirty years and counting. *Curr. Opin. Cell Biol.* 2009; 21:140–146. [PubMed: 19269802]
- Tonks NK. Protein tyrosine phosphatases: from genes to function, to disease. *Nat. Rev. Mol. Cell Biol.* 2006; 7:833–846. [PubMed: 17057753]
- Cohen P, Alessi DR. Kinase Drug Discovery - What's Next in the Field? *ACS Chem. Biol.* 2013; 8:96–104. [PubMed: 23276252]
- Zhang Z-Y. Protein Tyrosine Phosphatases: Prospects for Therapeutics. *Curr. Opin. Chem. Biol.* 2001; 5:416–423. [PubMed: 11470605]
- Julien SG, Dubé N, Hardy S, Tremblay ML. Inside the human cancer tyrosine phosphatome. *Nat. Rev. Cancer.* 2011; 11:35–49. [PubMed: 21179176]
- Cohen S, Dadi H, Shaoul E, Sharfe N, Roifman CM. Cloning and characterization of a lymphoid-specific, inducible human protein tyrosine phosphatase, Lyp. *Blood.* 1999; 93:2013–2024. [PubMed: 10068674]
- Gjorloff-Wingren A, Saxena M, Williams S, Hammi D, Mustelin T. Characterization of TCR-induced receptor-proximal signaling events negatively regulated by the protein tyrosine phosphatase PEP. *Eur. J. Immunol.* 1999; 29:3845–3854. [PubMed: 10601992]
- Cloutier J-F, Veillette A. Cooperative inhibition of T-cell antigen receptor signaling by a complex between a kinase and a phosphatase. *J. Exp. Med.* 1999; 189:111–121. [PubMed: 9874568]
- Wu J, Katrekar A, Honigberg LA, Smith AM, Conn MT, Tang J, Jeffery D, Mortara K, Sampang J, Williams SR, Buggy J, Clark JM. Identification of substrates of human protein-tyrosine phosphatase PTPN22. *J. Biol. Chem.* 2006; 281:11002–11010. [PubMed: 16461343]
- Bottini N, Musumeci L, Alonso A, Rahmouni S, Nika K, Rostamkhani M, MacMurray J, Meloni GF, Lucarelli P, Pellicchia M, Eisenbarth GS, Comings D, Mustelin T. A functional variant of lymphoid tyrosine phosphatase is associated with type I diabetes. *Nat. Genet.* 2004; 36:337–338. [PubMed: 15004560]
- Begovich AB, Carlton VE, Honigberg LA, Schrodi SJ, Chokkalingam AP, Alexander HC, Ardlie KG, Huang Q, Smith AM, Spoerke JM, Conn MT, Chang M, Chang SY, Saiki RK, Catanese JJ, Leong DU, Garcia VE, McAllister LB, Jeffery DA, Lee AT, Batliwalla F, Remmers E, Criswell

- LA, Seldin MF, Kastner DL, Amos CI, Sninsky JJ, Gregersen PK. A missense single-nucleotide polymorphism in a gene encoding a protein tyrosine phosphatase (PTPN22) is associated with rheumatoid arthritis. *Am. J. Hum. Genet.* 2004; 75:330–337. [PubMed: 15208781]
12. Carlton VE, Hu X, Chokkalingam AP, Schrodi SJ, Brandon R, Alexander HC, Chang M, Catanese JJ, Leong DU, Ardlie KG, Kastner DL, Seldin MF, Criswell LA, Gregersen PK, Beasley E, Thomson G, Amos CI, Begovich AB. PTPN22 genetic variation: evidence for multiple variants associated with rheumatoid arthritis. *Am. J. Hum. Genet.* 2005; 77:567–581. [PubMed: 16175503]
  13. Smyth D, Cooper JD, Collins JE, Heward JM, Franklyn JA, Howson JM, Vella A, Nutland S, Rance HE, Maier L, Barratt BJ, Guja C, Ionescu-Tirgoviste C, Savage DA, Dunger DB, Widmer B, Strachan DP, Ring SM, Walker N, Clayton DG, Twells RC, Gough SC, Todd JA. Replication of an association between the lymphoid tyrosine phosphatase locus (LYP/PTPN22) with type 1 diabetes, and evidence for its role as a general autoimmunity locus. *Diabetes.* 2004; 53:3020–3023. [PubMed: 15504986]
  14. Kyogoku C, Langefeld CD, Ortmann WA, Lee A, Selby S, Carlton VE, Chang M, Ramos P, Baechler EC, Batliwalla FM, Novitzke J, Williams AH, Gillett C, Rodine P, Graham RR, Ardlie KG, Gaffney PM, Moser KL, Petri M, Begovich AB, Gregersen PK, Behrens TW. Genetic association of the R620W polymorphism of protein tyrosine phosphatase PTPN22 with human SLE. *Am. J. Hum. Genet.* 2004; 75:504–507. [PubMed: 15273934]
  15. Vandiedonck C, Capdevielle C, Giraud M, Krumeich S, Jais JP, Eymard B, Tranchant C, Gajdos P, Garchon HJ. Association of the PTPN22\*R620W polymorphism with autoimmune myasthenia gravis. *Ann. Neurol.* 2006; 59:404–407. [PubMed: 16437561]
  16. Greve B, Hoffmann P, Illes Z, Rozsa C, Berger K, Weissert R, Melms A. The autoimmunity-related polymorphism PTPN22 1858C/T is associated with anti-titin antibodypositive myasthenia gravis. *Hum. Immunol.* 2009; 70:540–542. [PubMed: 19406179]
  17. Canton I, Akhtar S, Gavalas NG, Gawkrödger DJ, Blomhoff A, Watson PF, Weetman AP, Kemp EH. A single-nucleotide polymorphism in the gene encoding lymphoid protein tyrosine phosphatase (PTPN22) confers susceptibility to generalised vitiligo. *Genes. Immun.* 2005; 6:584–587. [PubMed: 16015369]
  18. LaBerge GS, Bennett DC, Fain PR, Spritz RA. PTPN22 is genetically associated with risk of generalized vitiligo, but CTLA4 is not. *J. Investig. Dermatol.* 2008; 128:1757–1762. [PubMed: 18200060]
  19. Burn GL, Svensson L, Sanchez-Blanco C, Saini M, Cope AP. Why is PTPN22 a good candidate susceptibility gene for autoimmune disease? *FEBS Lett.* 2011; 585:3689–3698. [PubMed: 21515266]
  20. Vang T, Congia M, Macis MD, Musumeci L, Orru V, Zavattari P, Nika K, Tautz L, Tasken K, Cucca F, Mustelin T, Bottini N. Autoimmune-associated lymphoid tyrosine phosphatase is a gain-of-function variant. *Nat. Genet.* 2005; 37:1317–1319. [PubMed: 16273109]
  21. Rieck M, Arechiga A, Onengut-Gumuscu S, Greenbaum C, Concannon P, Buckner JH. Genetic variation in PTPN22 corresponds to altered function of T and B lymphocytes. *J. Immunol.* 2007; 179:4704–4710. [PubMed: 17878369]
  22. Arechiga AF, Habib T, He Y, Zhang X, Zhang Z-Y, Funk A, Buckner JH. Cutting edge: the PTPN22 allelic variant associated with autoimmunity impairs B cell signaling. *J. Immunol.* 2009; 182:3343–3347. [PubMed: 19265110]
  23. Habib T, Funk A, Rieck M, Brahmandam A, Dai X, Panigrahi AK, Luning Prak ET, Meyer-Bahlburg A, Sanda S, Greenbaum C, Rawlings DJ, Buckner JH. Altered B cell homeostasis is associated with type I diabetes and carriers of the PTPN22 allelic variant. *J Immunol.* 2012; 188:487–496. [PubMed: 22105996]
  24. Vang T, Liu WH, Delacroix L, Wu S, Vasile S, Dahl R, Yang L, Musumeci L, Francis D, Landskron J, Tasken K, Tremblay ML, Lie BA, Page R, Mustelin T, Rahmouni S, Rickert RC, Tautz L. LYP inhibits T-cell activation when dissociated from CSK. *Nat. Chem. Biol.* 2012; 8:437–446. [PubMed: 22426112]
  25. Orrú V, Tsai SJ, Rueda B, Fiorillo E, Stanford SM, Dasgupta J, Hartiala J, Zhao L, Ortego-Centeno N, D'Alfonso S, Italian Collaborative Group, Arnett FC, Wu H, Gonzalez-Gay MA, Tsao BP, Pons-Estel B, Alarcon-Riquelme ME, He Y, Zhang Z-Y, Allayee H, Chen XS, Martin J,

- Bottini N. A loss-of-function variant of PTPN22 is associated with reduced risk of systemic lupus erythematosus. *Hum. Mol. Genet.* 2009; 18:569–579. [PubMed: 18981062]
26. Brownlie RJ, Miosge LA, Vassilakos D, Svensson LM, Cope A, Zamoyska R. Lack of the phosphatase PTPN22 increases adhesion of murine regulatory T cells to improve their immunosuppressive function. *Sci Signal.* 2013; 5:ra87. [PubMed: 23193160]
27. Zheng P, Kissler S. PTPN22 Silencing in the NOD Model Indicates the Type 1 Diabetes-Associated Allele Is Not a Loss-of-Function Variant. *Diabetes.* 2012; 62:896–904. [PubMed: 23193190]
28. Yu X, Sun JP, He Y, Guo XL, Liu S, Zhou B, Hudmon A, Zhang Z-Y. Structure, inhibitor, and regulatory mechanism of Lyp, a lymphoid-specific tyrosine phosphatase implicated in autoimmune diseases. *Proc. Natl. Acad. Sci. USA.* 2007; 104:19767–19772. [PubMed: 18056643]
29. Xie YL, Liu YD, Gong GL, Rinderspacher A, Deng SX, Smith DH, Toebben U, Tzilianos E, Branden L, Vidovic D, Chung C, Schurer S, Tautz L, Landry DW. Discovery of a novel submicromolar inhibitor of the lymphoid specific tyrosine phosphatase. *Bioorg. Med. Chem. Lett.* 2008; 18:2840–2844. [PubMed: 18434147]
30. Wu S, Bottini M, Rickert RC, Mustelin T, Tautz L. In silico screening for PTPN22 inhibitors: active hits from an inactive phosphatase conformation. *ChemMedChem.* 2009; 4:440–444. [PubMed: 19177473]
31. Karver MR, Krishnamurthy D, Kulkarni RA, Bottini N, Barrios AM. Identifying potent selective protein tyrosine phosphatase inhibitors from a library of Au(I) complexes. *J. Med. Chem.* 2009; 52:6912–6918. [PubMed: 19888762]
32. Karver MR, Krishnamurthy D, Bottini N, Barrios AM. Gold(I) phosphine mediated selective inhibition of lymphoid tyrosine phosphatase. *J. Inorg. Biochem.* 2010; 104:268–273. [PubMed: 20083307]
33. Vidovi D, Xie Y, Rinderspacher A, Deng SX, Landry DW, Chung C, Smith DH, Tautz L, Schürer SC. Distinct functional and conformational states of the human lymphoid tyrosine phosphatase catalytic domain can be targeted by choice of the inhibitor chemotype. *J. Comput. Aided. Mol. Des.* 2011; 25:873–883. [PubMed: 21904909]
34. Stanford SM, Krishnamurthy D, Falk MD, Messina R, Debnath B, Li S, Liu T, Kazemi R, Dahl R, He Y, Yu X, Chan AC, Zhang Z-Y, Barrios AM, Woods VL Jr, Neamati N, Bottini N. Discovery of a novel series of inhibitors of lymphoid tyrosine phosphatase with activity in human T cells. *J. Med. Chem.* 2011; 54:1640–1654. [PubMed: 21341673]
35. Vang T, Xie Y, Liu WH, Vidovi D, Liu Y, Wu S, Smith DH, Rinderspacher A, Chung C, Gong G, Mustelin T, Landry DW, Rickert RC, Schürer SC, Deng SX, Tautz L. Inhibition of lymphoid tyrosine phosphatase by benzofuran salicylic acids. *J. Med. Chem.* 2011; 54:562–571. [PubMed: 21190368]
36. He Y, Zeng L-F, Yu Z-H, He R, Liu S, Zhang Z-Y. Bicyclic benzofuran and indole-based salicylic acids as protein tyrosine phosphatase inhibitors. *Bioorg. Med. Chem.* 2012; 20:1940–1946. [PubMed: 22133902]
37. Puius YA, Zhao Y, Sullivan M, Lawrence DS, Almo SC, Zhang Z-Y. Identification of a Second Aryl Phosphate-Binding Site in Protein-Tyrosine Phosphatase 1B: A Paradigm for Inhibitor Design. *Proc. Natl. Acad. Sci. USA.* 1997; 94:13420–13425. [PubMed: 9391040]
38. Zhang Z-Y. Protein Tyrosine Phosphatases: Structure and function Substrate Specificity and Inhibitor Development. *Annu. Rev. Pharmacol. Toxicol.* 2002; 42:209–234. [PubMed: 11807171]
39. He Y, Xu J, Yu Z-H, Gunawan AM, Wu L, Wang L, Zhang Z-Y. Discovery and evaluation of novel inhibitors of Mycobacterium protein tyrosine phosphatase B from the 6-hydroxy-benzofuran-5-carboxylic acid scaffold. *J. Med. Chem.* 2013; 56:832–842. [PubMed: 23305444]
40. Barr AJ, Ugochukwu E, Lee WH, King ON, Filippakopoulos P, Alfano I, Savitsky P, Burgess-Brown NA, Muller S, Knapp S. Large-scale structural analysis of the classical human protein tyrosine phosphatome. *Cell.* 2009; 136:352–363. [PubMed: 19167335]
41. Sarmiento M, Wu L, Keng YF, Song L, Luo Z, Huang Z, Wu G-Z, Yuan AK, Zhang Z-Y. Structure-based discovery of small molecule inhibitors targeted to protein tyrosine phosphatase 1B. *J. Med. Chem.* 2000; 43:146–155. [PubMed: 10649970]



42. Liang F, Huang Z, Lee S-Y, Liang J, Ivanov MI, Alonso A, Bliska JB, Lawrence DS, Mustelin T, Zhang Z-Y. Aurintricarboxylic acid blocks in vitro and in vivo activity of YopH, an essential virulent factor of *Yersinia pestis*, the agent of plague. *J. Biol. Chem.* 2003; 278:41734–41741. [PubMed: 12888560]
43. Zhang X, He Y, Liu S, Yu Z, Jiang Z-X, Yang Z, Dong Y, Nabinger SC, Wu L, Gunawan AM, Wang L, Chan RJ, Zhang Z-Y. Salicylic acid-based small molecule inhibitor for the oncogenic Src homology-2 domain containing protein tyrosine phosphatase-2 (SHP2). *J. Med. Chem.* 2010; 53:2482–2493. [PubMed: 20170098]
44. Sarmiento M, Puius YA, Vetter SW, Keng YF, Wu L, Zhao Y, Lawrence DS, Almo SC, Zhang Z-Y. Structural basis of plasticity in protein tyrosine phosphatase 1B substrate recognition. *Biochemistry.* 2000; 39:8171–8179. [PubMed: 10889023]
45. Bottini N, Vang T, Cucca F, Mustelin T. Role of PTPN22 in type 1 diabetes and other autoimmune diseases. *Semin. Immunol.* 2006; 18:207–213. [PubMed: 16697661]
46. Cosulich ME, Rubartelli A, Risso A, Cozzolino F, Bargellesi A. Functional characterization of an antigen involved in an early step of T-cell activation. *Proc. Natl. Acad. Sci. USA.* 1987; 84:4205–4209. [PubMed: 3295878]
47. Moran AE, Holzappel KL, Xing Y, Cunningham NR, Maltzman JS, Punt J, Hogquist KA. T cell receptor signal strength in Treg and iNKT cell development demonstrated by a novel fluorescent reporter mouse. *J. Exp. Med.* 2011; 208:1279–1289. [PubMed: 21606508]
48. Peavy RD, Metcalfe DD. Understanding the mechanisms of anaphylaxis. *Curr. Opin. Allergy Clin Immunol.* 2008; 8:310–315. [PubMed: 18596587]
49. Bischoff SC. Role of mast cells in allergic and non-allergic immune responses: comparison of human and murine data. *Nat. Rev. Immunol.* 2007; 7:93–104. [PubMed: 17259966]
50. Griffiths GM. Secretory lysosomes - a special mechanism of regulated secretion in haemopoietic cells. *Trends Cell Biol.* 1996; 6:329–332. [PubMed: 15157429]
51. Obiri DD, Flink N, Maier JV, Neeb A, Maddalo D, Thiele W, Menon A, Stassen M, Kulkarni RA, Garabedian MJ, Barrios AM, Cato AC. PEST-domain-enriched tyrosine phosphatase and glucocorticoids as regulators of anaphylaxis in mice. *Allergy.* 2012; 67:175–182. [PubMed: 21981059]
52. Gilfillan, AM.; Metcalfe, DD.; Austin, SJ. Mast cell biology: Introduction and overview. In: Gilfillan, AM.; Metcalfe, DD., editors. *Mast cell biology: Contemporary and emerging topics.* Austin, TX: Landes Bioscience; 2011. p. 2-13.
53. Schorpp M, Jager R, Schellander K, Schenkel J, Wagner EF, Weiher H, Angel P. The human ubiquitin C promoter directs high ubiquitous expression of transgenes in mice. *Nucleic Acids Res.* 1996; 24:1787–1788. [PubMed: 8650001]
54. Spurg A, Waldvogel SR. High-Yielding Cleavage of (Aryloxy)acetates. *Eur. J. Org. Chem.* 2008; 2008:337–342.
55. Minor W, Cymborowski M, Otwinowski Z, Chruszcz M. HKL-3000: the integration of data reduction and structure solution--from diffraction images to an initial model in minutes. *Acta Crystallogr. D.* 2006; 62:859–866. [PubMed: 16855301]
56. Navaza J. AMoRe: an automated package for molecular replacement. *Acta Crystallogr. A.* 1994; 50:157–163.
57. Brünger AT, Adams PD, Clore GM, DeLano WL, Gros P, Grosse-Kunstleve RW, Jiang JS, Kuszewski J, Nilges M, Pannu NS, Read RJ, Rice LM, Simonson T, Warren GL. Crystallography & NMR system: a new software suite for macromolecular structure determination. *Acta Crystallogr. D. Biol. Crystallogr.* 1998; 54:905–921. [PubMed: 9757107]
58. Brünger AT. Free R value: a novel statistical quantity for assessing the accuracy of crystal structures. *Nature.* 1992; 355:472–475. [PubMed: 18481394]
59. Jones TA, Zou JY, Cowan SW, Kjeldgaard M. Improved methods for building protein models in electron density maps and the location of errors in these models. *Acta Crystallogr. A.* 1991; 47:110–119. [PubMed: 2025413]
60. Shaw JP, Utz PJ, Durand DB, Toole JJ, Emmel EA, Crabtree GR. Identification of a putative regulator of early T cell activation genes. *Science.* 1988; 241:202–205. [PubMed: 3260404]

61. Kassel O, Sancono A, Krätzschar J, Kreft B, Stassen M, Cato AC. Glucocorticoids inhibit MAP kinase via increased expression and decreased degradation of MKP-1. *EMBO J.* 2001; 20:7108–7116. [PubMed: 11742987]
62. Weiss A, Stobo JD. Requirement for the coexpression of T3 and the T cell antigen receptor on a malignant human T cell line. *J. Exp. Med.* 1984; 160:1284–1299. [PubMed: 6208306]
63. Hasegawa K, Martin F, Huang G, Tumas D, Diehl L, Chan AC. PEST domain-enriched tyrosine phosphatase (PEP) regulation of effector/memory T cells. *Science.* 2004; 303:685–689. [PubMed: 14752163]
64. Maier JV, Brema S, Tuckermann J, Herzer U, Klein M, Stassen M, Moorthy A, Cato AC. Dual specificity phosphatase 1 knockout mice show enhanced susceptibility to anaphylaxis but are sensitive to glucocorticoids. *Mol. Endocrinol.* 2007; 21:2663–2671. [PubMed: 17636038]

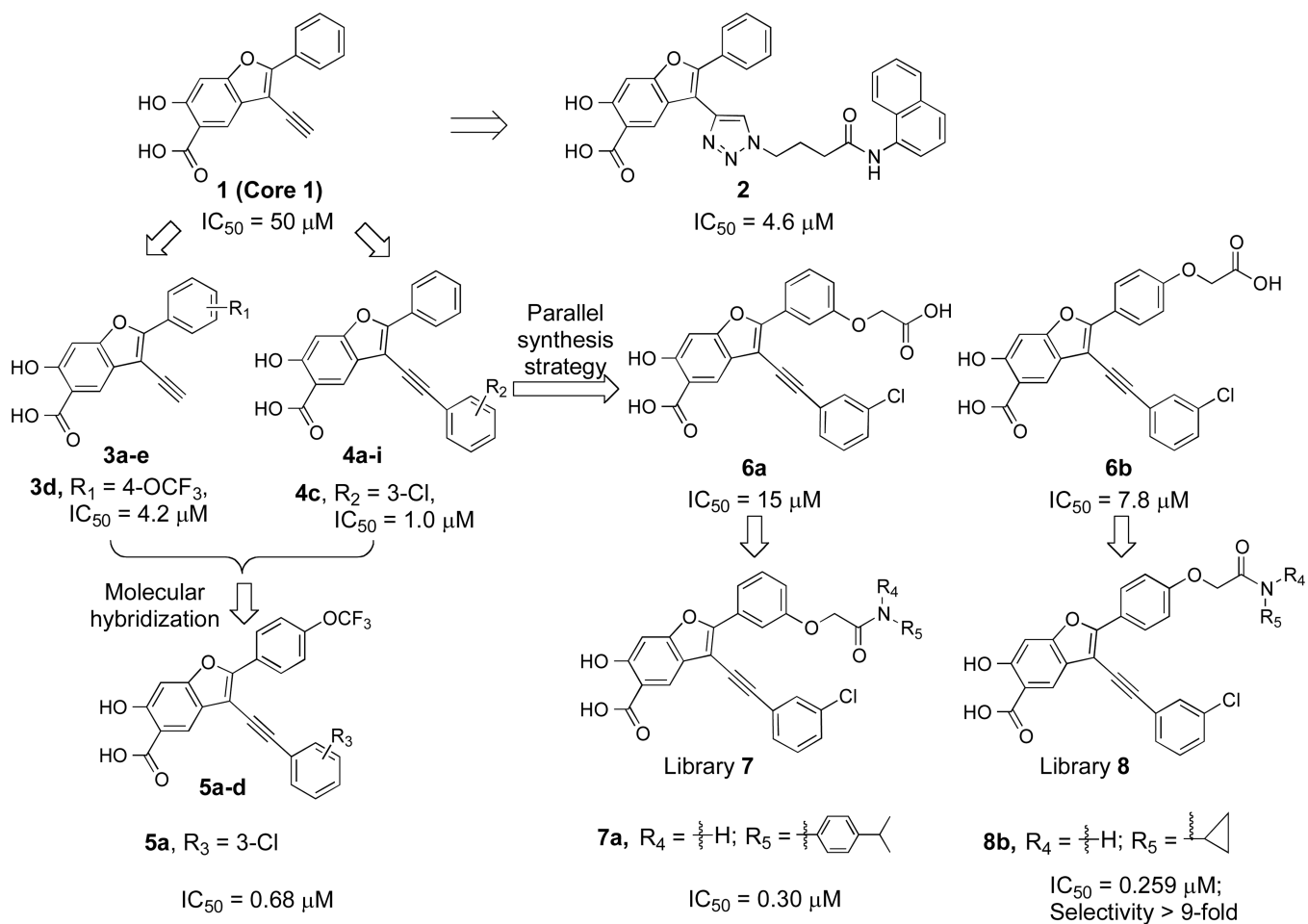
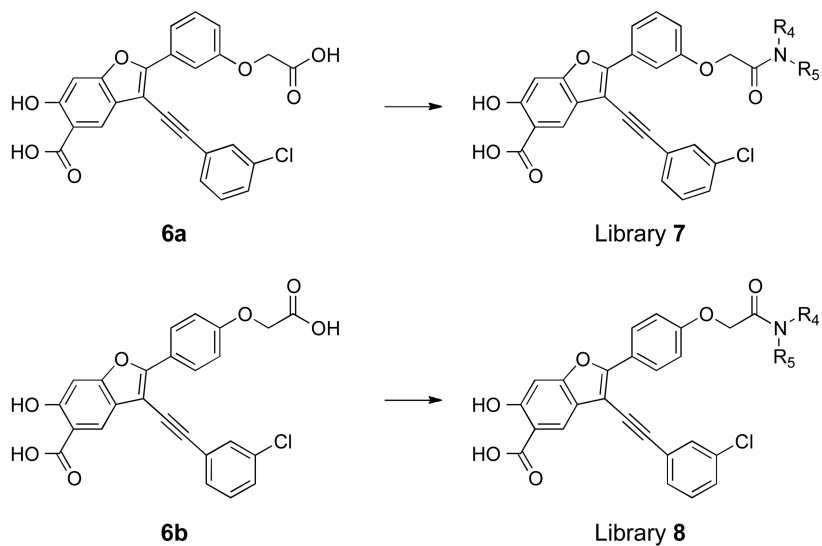


**Figure 1.** A structure-based focused library approach transforms the 6-hydroxy-benzofuran-5-carboxylic acid Core **1** into the highly potent and selective LYP inhibitor **8b**.



#### $R_4R_5NH$ : Amines used for library construction

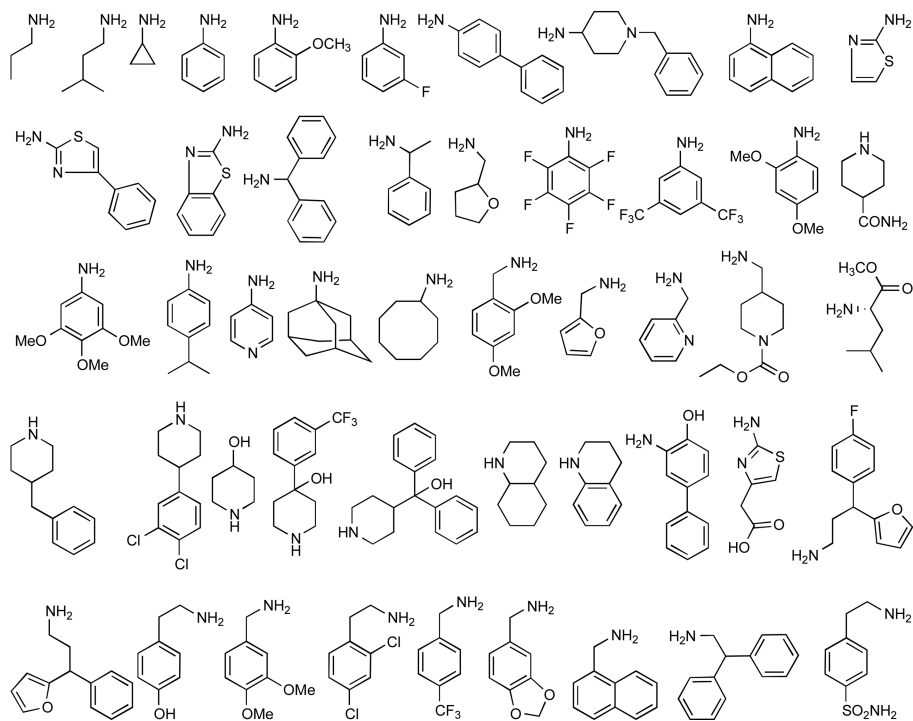


**Figure 2.** The preparation of libraries **7** and **8** using amide chemistry. The structures of the starting compounds **6a** and **6b** as well as the structures of the 48 amines are shown.

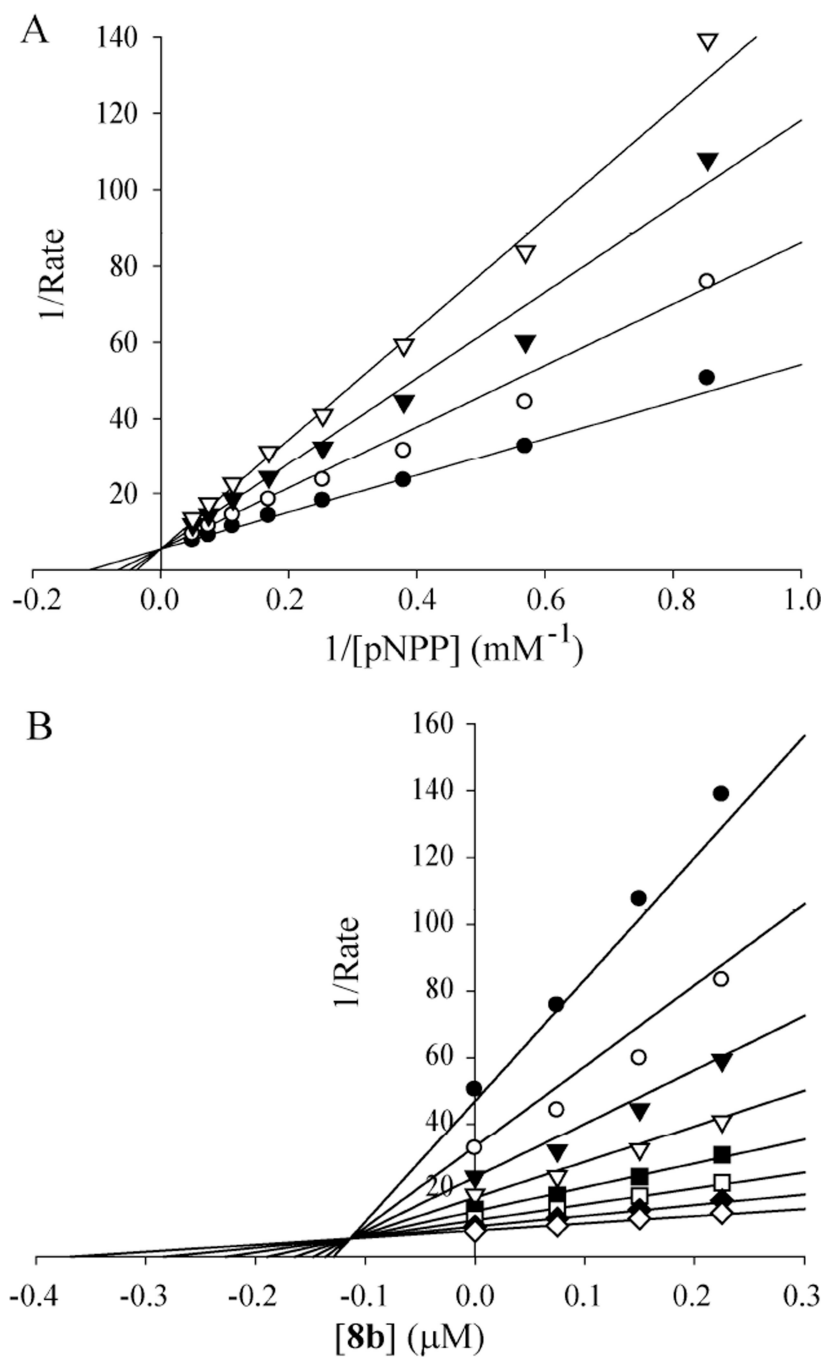


**Figure 3.** Lineweaver-Burk plot (A) and Dixon plot (B) for compound **8b**-mediated LYP inhibition using *p*NPP as a substrate. *p*NPP concentrations were 1.17, 1.76, 2.63, 3.95, 5.93, 8.89, 13.3, and 20 mM. Compound **8b** concentrations were 0 (•), 75 (μ), 150 (τ), and 225 (∇) nM, respectively.

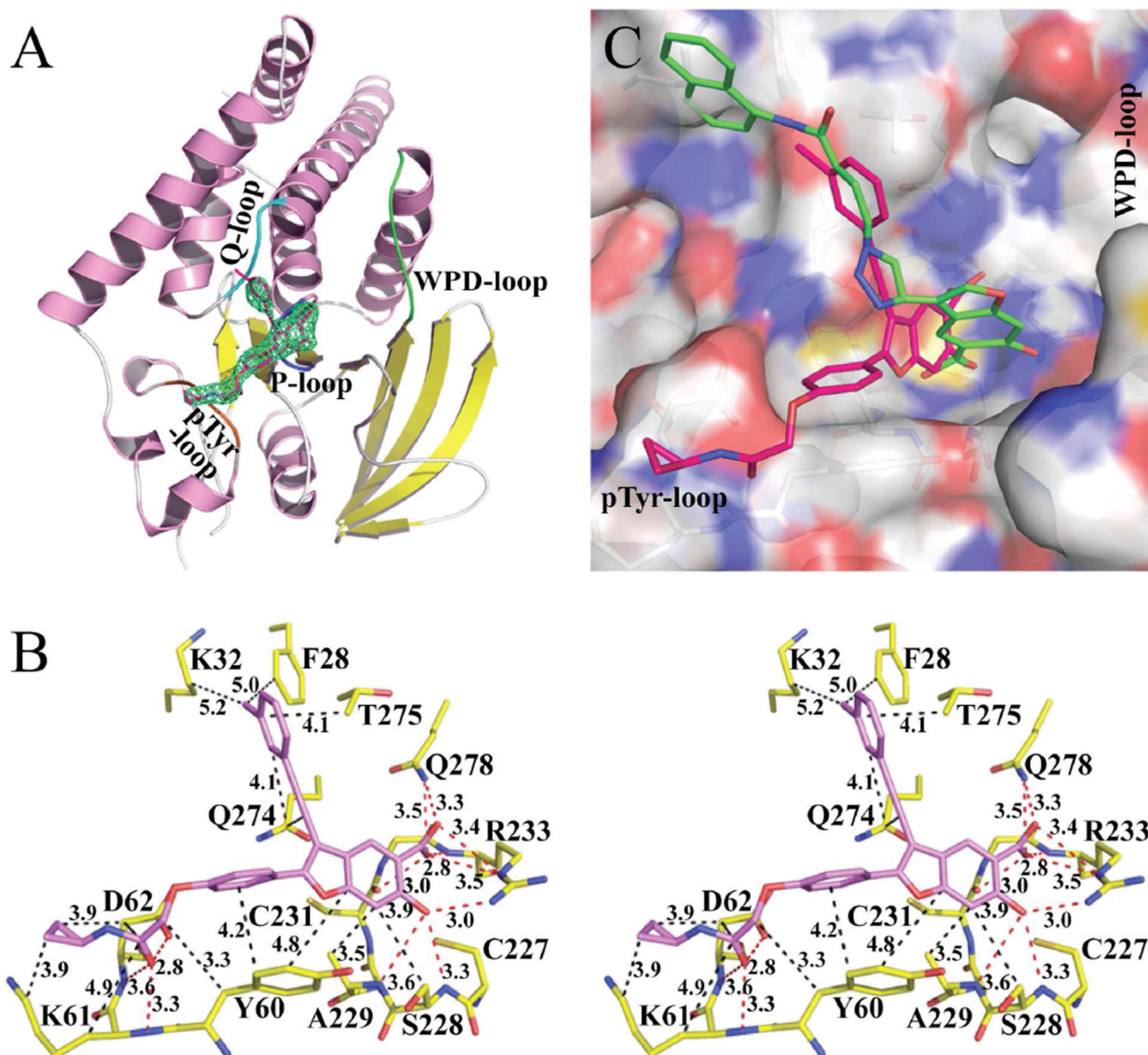


**Figure 4.** Crystal structure of LYP in complex with compound **8b**. (A). Overall structure of LYP catalytic domain in complex with **8b**.  $\alpha$  helices and  $\beta$  strands are colored in pink and yellow, respectively. The P-loop is shown in blue, the WPD-loop in green, the Q-loop in cyan, and the pTyr-loop in orange. Compound **8b** is shown in stick model with unbiased  $F_o - F_c$  map contoured at  $3.0\sigma$  calculated before the ligand and water molecules were added to the model. (B). Detailed interactions between compound **8b** and LYP. Polar interactions or H-bonds are shown by red dashed lines; hydrophobic interactions are shown in black dashed lines. Residues involved in polar or hydrophobic interactions are shown with a cutoff distance of 3.6 and 5.2 Å, respectively. (C). Binding mode comparison between compound **8b** and compound **2**. The superposition of LYP•**8b** and LYP•**2** was calculated with active site residues without the ligands. LYP active site was shown by transparent surface representation, and the key residues are depicted in stick model. Atomic colors were as

follows: oxygen – red, carbon – white, sulfur – orange, and nitrogen – blue. Carbon atoms of **8b** were colored red, and compound **2**'s carbon atoms were colored green. For **2**, the phenyl ring on the 2-position of the benzofuran core was invisible in the crystal structure.

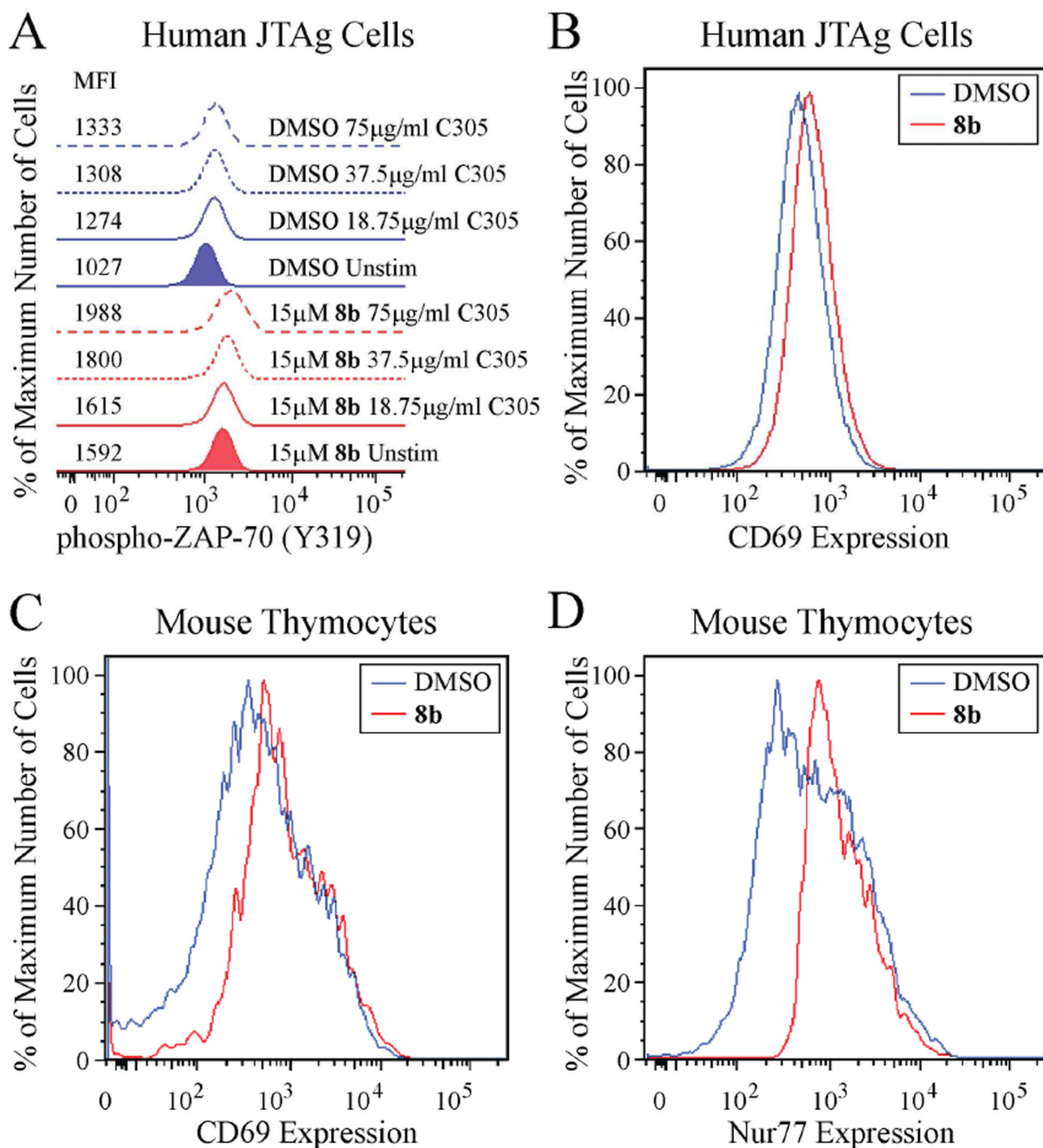
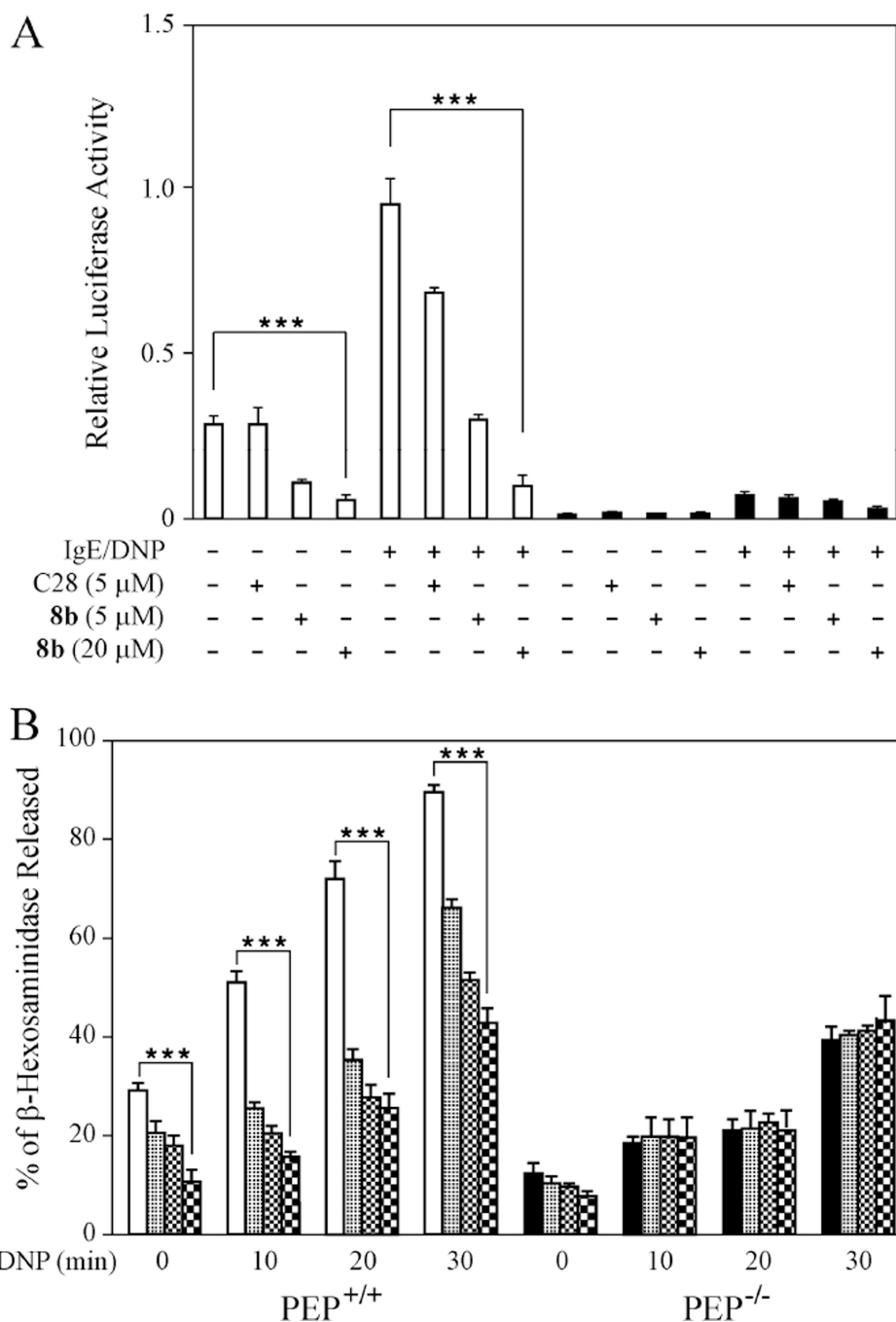


**Figure 5.**






The LYP inhibitor **8b** increases T cell activation. (A) Compound **8b** increases activation of ZAP-70 in human T cells. JTAG cells were pre-incubated with 15  $\mu$ M **8b** (red graphs) or DMSO alone (blue graphs) for 30 min at 37°C, followed by stimulation with increasing concentrations of C305 supernatant (18.75  $\mu$ g/ml, solid lines; 37.5  $\mu$ g/ml, dashed lines; 75  $\mu$ g/ml, long-dashed lines) or left unstimulated (shaded graphs) for 2 min at 37°C. Graphs show cell fluorescence after staining with an AlexaFluor-488-conjugated anti-phospho-ZAP-70 (Y319) antibody. Median fluorescence intensity (MFI) of each sample is shown. (B) Compound **8b** increases CD69 expression on human T cells. JTAG cells were incubated



with 15  $\mu\text{M}$  **8b** (red graph, MFI=616) or DMSO alone (blue graph, MFI=451) for 4.5 hours at 37°C. Graphs show cell fluorescence after staining with a FITC-conjugated anti-CD69 antibody. (C–D) Compound **8b** increases the activation of primary mouse T cells. Thymocytes from Nur77<sup>GFP</sup> mice were incubated with 15  $\mu\text{M}$  **8b** (red graph) or DMSO alone (blue graph) for 3.5 hours at 37°C. (C) Graphs show cell fluorescence after staining with a FITC-conjugated anti-CD69 antibody (MFI of **8b**-treated sample=758; MFI of DMSO-treated sample=381). (D) Graphs show Nur77 expression as assessed by GFP cell fluorescence (MFI of **8b**-treated sample=1120; MFI of DMSO-treated sample=604). Histograms from all **8b**-treated samples in this figure were assessed compared to histograms from the respective DMSO-treated samples using the Kolmogorov-Smirnov test, and the distributions were found to be distinct with 99.9% confidence. Data in this figure are representative of 2 independent experiments with similar results.



**Figure 6.** Effects of compound **8b** in mast cells. (A) Compound **8b** decreases NF-AT luciferase activity in BMMC.  $8 \times 10^6$  cells PEP<sup>+/+</sup> and PEP<sup>-/-</sup> BMMC were transfected with 4.5 μg 3xNF-AT-luciferase and 0.8 μg of Renilla luciferase expression. 24 h after transfection, the cells were sensitized with anti-DNP IgE for 18 h. Cells were treated with C28 (5 μM) or **8b** (5 μM, 20 μM) for 1 h to the end of IgE incubation. Cells were then activated with DNP-HSA (200 ng/ml) for 8 h and firefly luciferase activity was measured and normalized to Renilla luciferase activity. Results are presented as the mean  $\pm$  SEM (n=3). PEP<sup>+/+</sup> ; PEP<sup>-/-</sup> . Results in bar charts are presented as the mean  $\pm$  SEM (\*\*\*)p 0.0001, n=3 (B).

Compound **8b** reduces mast cell degranulation in BMMC.  $5 \times 10^6$  cells/ml BMMC from PEP<sup>+/+</sup> and PEP<sup>-/-</sup> mice were sensitized with anti-DNP-IgE for 16 h and treated with C28 (5  $\mu$ M), **8b** (5  $\mu$ M) or **8b** (20  $\mu$ M) for 1 h at the end of IgE incubation. These cells were then activated with DNP-HSA(200 ng/ml) for various time points. BMMC were pelleted and the amount of  $\beta$ -hexosaminidase in the supernatant and in the solubilized pellet were measured using p-nitrophenyl N-acetyl- $\beta$ -D-glucosaminidase (p-NAG) as a substrate. Percent degranulation was calculated as follows: (released activity/total activity)  $\times$  100. The results are represented as the mean of  $\pm$  SEM of 3 independent experiments (\*\*p 0.0005, n=3). PEP<sup>+/+</sup> ; PEP<sup>-/-</sup> ; C28 (5 $\mu$ M) ; **8b** (5 $\mu$ M) ; **8b** (20 $\mu$ M) . The statistics were calculated using unpaired, 2-tailed, Student's t-test.

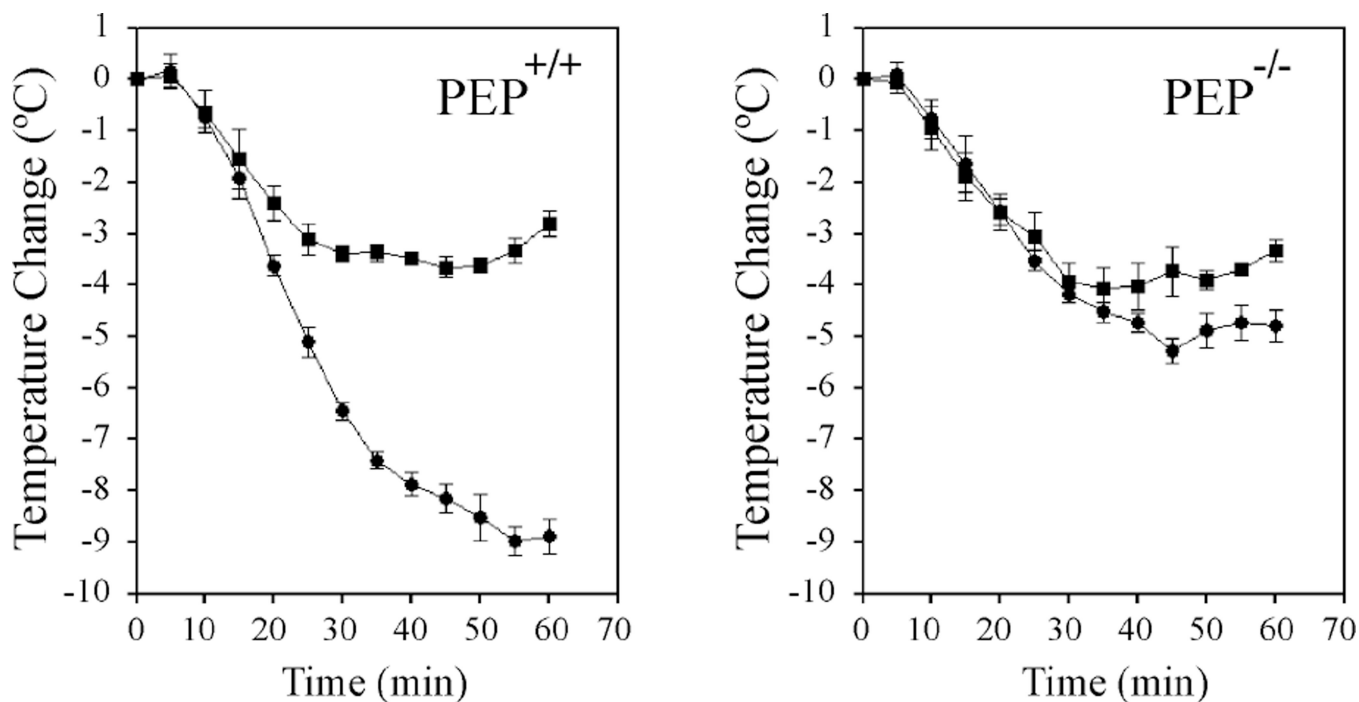


**Figure 7.**

Inhibition of anaphylaxis by compound **8b**. PEP<sup>+/+</sup> and PEP<sup>-/-</sup> mice were sensitized for 24 h with 1 mg/kg IgE and subsequently injected intra-peritoneal (IP) with either vehicle alone (PBS, 1 mg/kg) or **8b** (20  $\mu$ M) for 1 h to the end of the IgE incubation time. Anaphylaxis was induced with intra-venous injection of 200  $\mu$ l DNP-HSA and the change in body temperatures measured every 5 min for 1h. Change in body temperature for PEP<sup>+/+</sup> and PEP<sup>-/-</sup> mice are shown in (•) (PBS) and (v) (**8b**) respectively. Results are presented as the mean  $\pm$  SEM. (n=5).

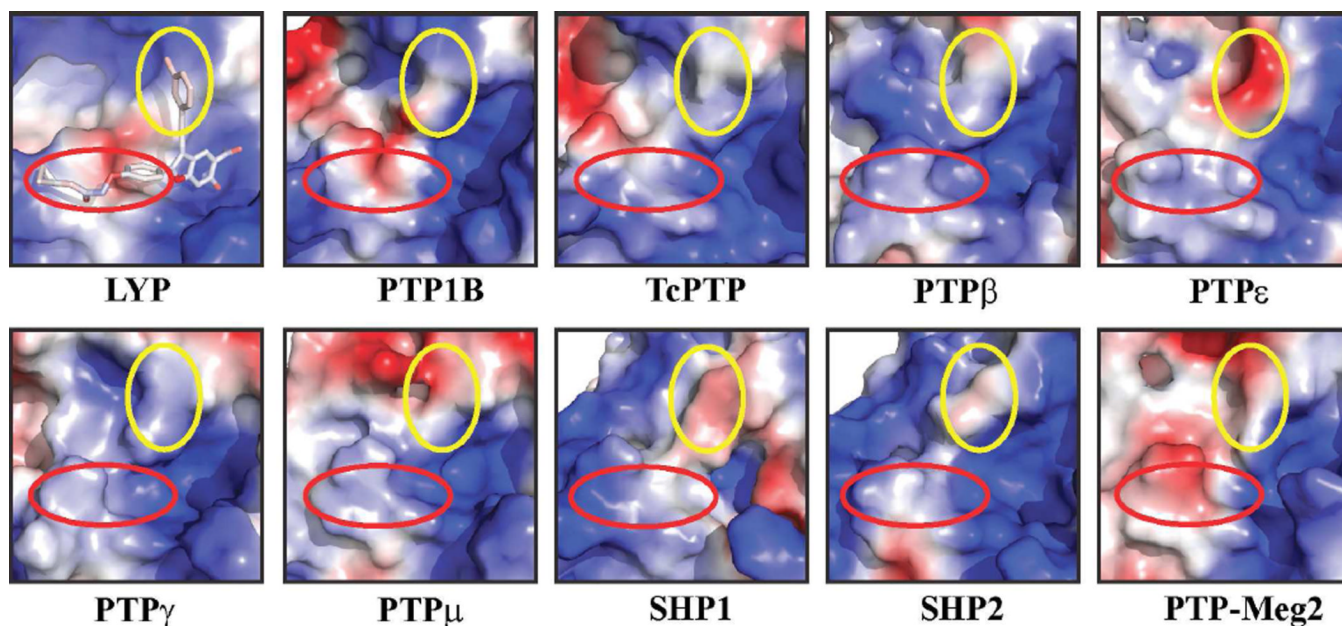
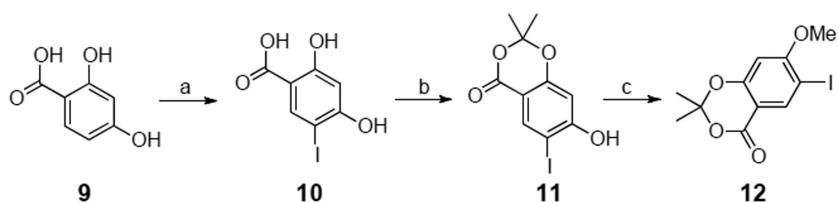
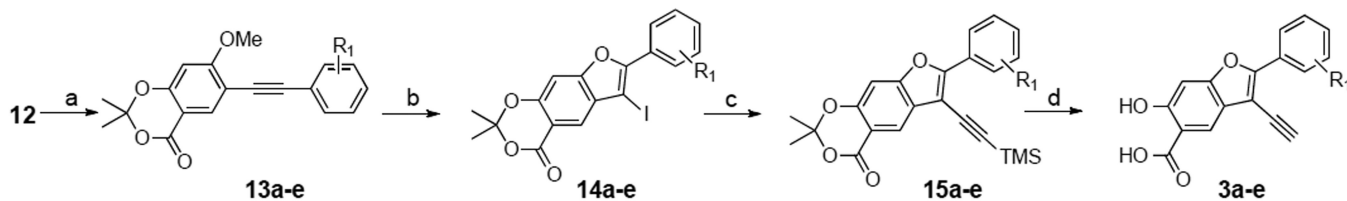


**Figure 8.**

Compound **8b** binding site comparison between LYP and other PTPs. The PTP active sites and the peripheral pockets are depicted by electrostatic surface representation prepared by PyMol (The PyMOL Molecular Graphics System, Version 1.4.1 Schrödinger, LLC.). The binding site for the substituted phenyl group at the 2-position of benzofuran ring was marked by a red circle, and the binding site for the 3-chlorophenyl ring attached to the 3-ethynyl group in the benzofuran ring was marked by a yellow circle. Compound **8b** is shown in stick model colored according to electrostatic properties of atoms.

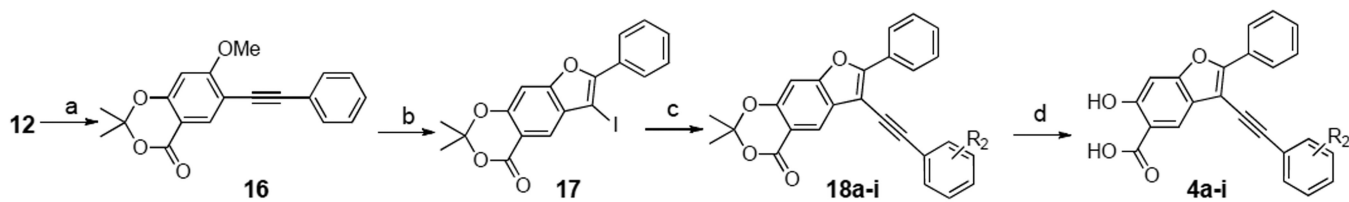


**Reaction Conditions:** a) ICl, AcOH, rt, 4 h, 92%; b) Acetone, TFAA, TFA, rt, 24 h, 50%; c) MeI, K<sub>2</sub>CO<sub>3</sub>, DMSO, rt, 4 h, 96%.



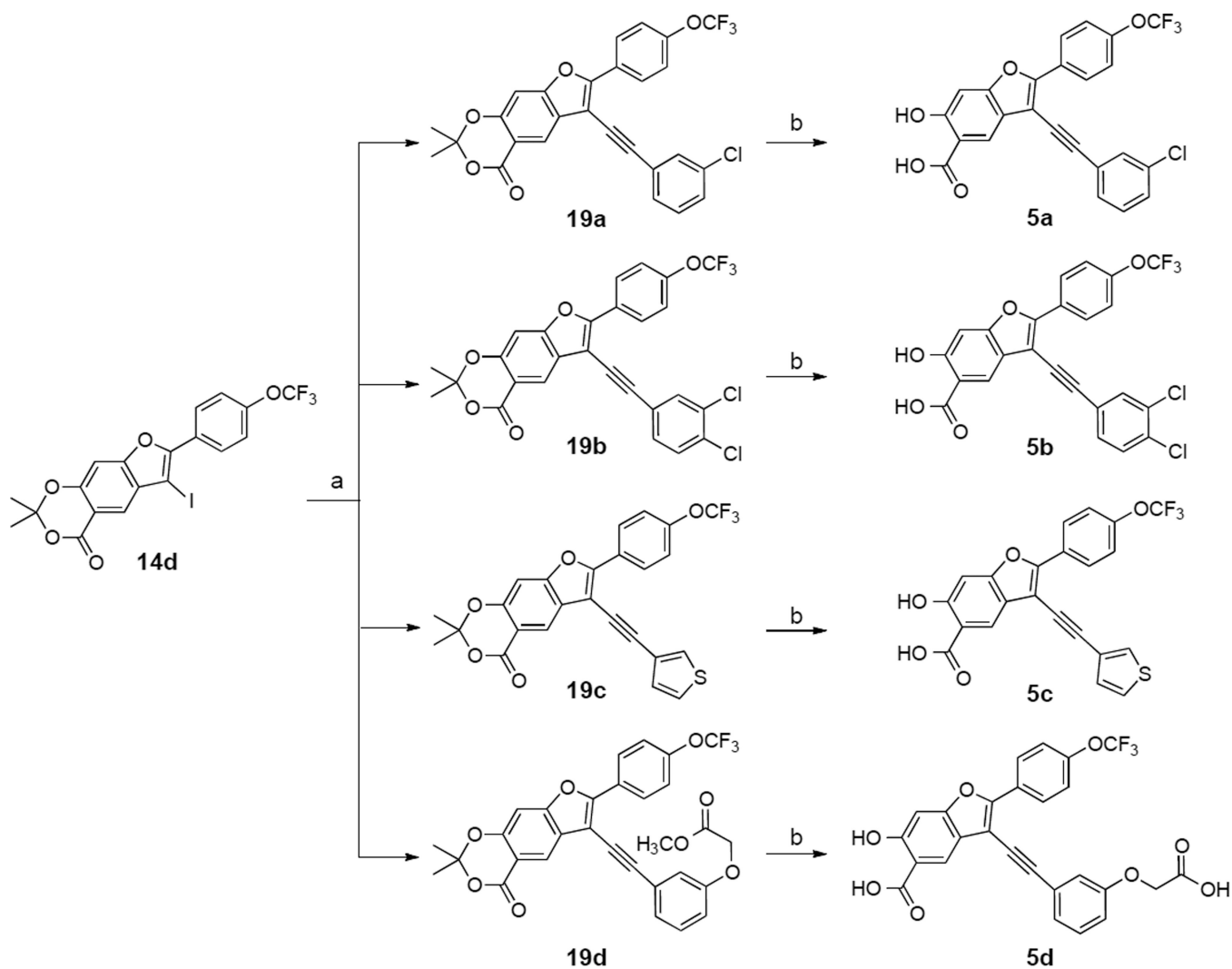
**Reaction Conditions:** a) Pd(PPh<sub>3</sub>)<sub>2</sub>Cl<sub>2</sub>, CuI, Et<sub>3</sub>N, rt, overnight, 70 - 90% b) I<sub>2</sub>, NaHCO<sub>3</sub>, MeCN, 70 °C, 24 h, 60-80%; c) Ethynyltrimethylsilane, Pd(PPh<sub>3</sub>)<sub>2</sub>Cl<sub>2</sub>, CuI, Et<sub>3</sub>N, rt, overnight, 70 - 90%; d) KOH, THF/H<sub>2</sub>O, reflux, 2h, 80 - 95%.

**Scheme 1.**  
Synthesis of compounds **3a-e**.



**Reaction Conditions:** a) Pd(PPh<sub>3</sub>)<sub>2</sub>Cl<sub>2</sub>, CuI, Et<sub>3</sub>N, rt, overnight, 76%; b) I<sub>2</sub>, NaHCO<sub>3</sub>, MeCN, 70 °C, 24 h, 65%; c) Pd(PPh<sub>3</sub>)<sub>2</sub>Cl<sub>2</sub>, CuI, Et<sub>3</sub>N, 40 °C, overnight, 70-80%; d) KOH, THF/H<sub>2</sub>O, reflux, 2 h, 80-95%

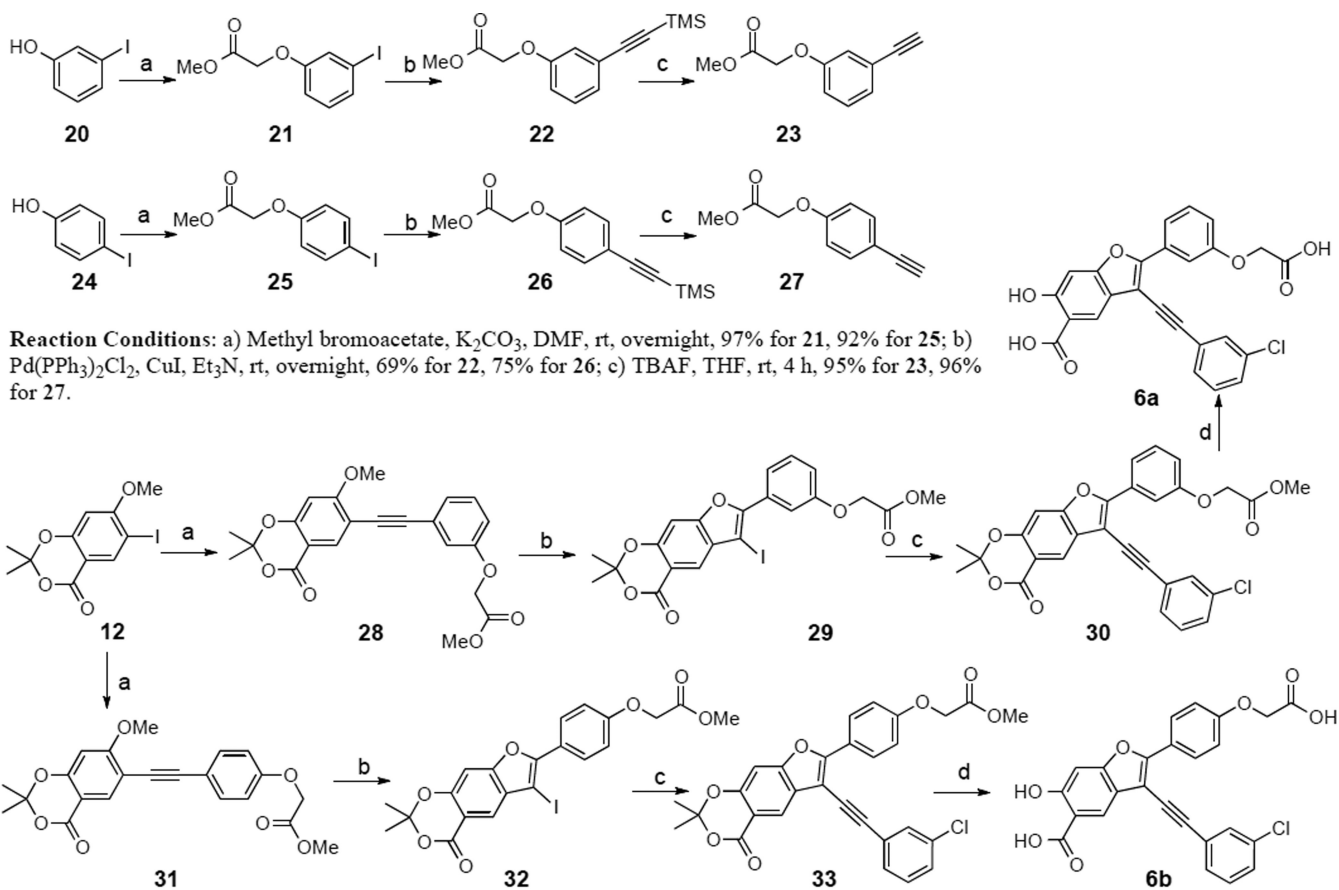
**Scheme 2.**  
Synthesis of compounds **4a-i**.



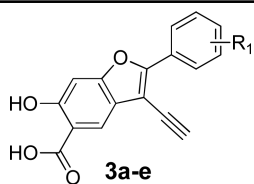
**Reaction Conditions:** a)  $\text{Pd}(\text{PPh}_3)_2\text{Cl}_2$ ,  $\text{CuI}$ ,  $\text{Et}_3\text{N}$ , rt, overnight, 70-80%; b)  $\text{KOH}$ ,  $\text{THF}/\text{H}_2\text{O}$ , reflux, 2 h, 80-95%.

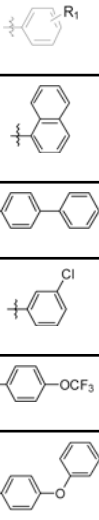
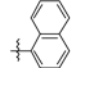
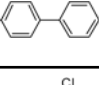
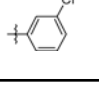
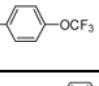
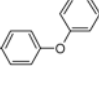
**Scheme 3.**  
Synthesis of compounds **5a-d**.

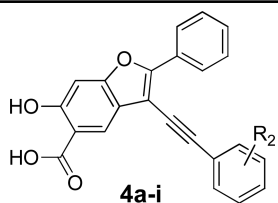




**Scheme 4.**  
Synthesis of compounds **6a** and **6b**.

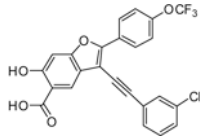
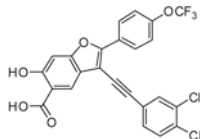
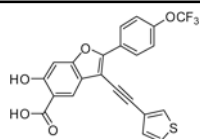
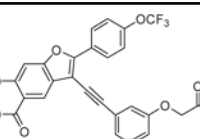
**Table 1***IC*<sub>50</sub> of Core **1**-based analogues (**3a–e**) against LYP.

Compd #		<i>IC</i> <sub>50</sub> (μM)
<b>3a</b>		8.4 ± 0.3
<b>3b</b>		1.82 ± 0.06
<b>3c</b>		10.0 ± 1
<b>3d</b>		4.2 ± 0.6
<b>3e</b>		5.2 ± 0.2

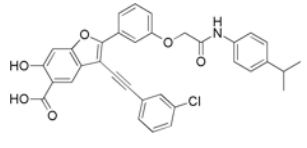
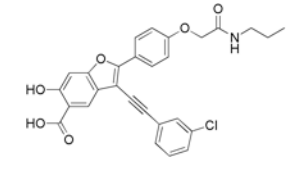
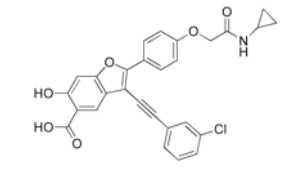
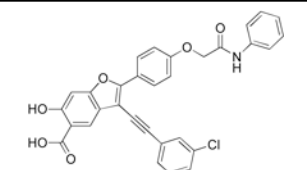
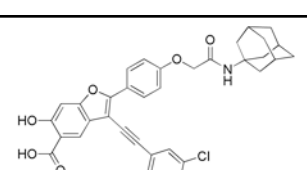
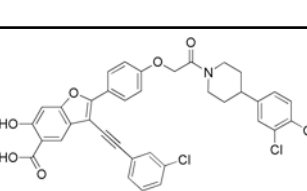
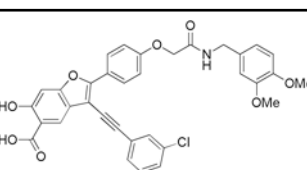
**Table 2***IC*<sub>50</sub> of Core **1**-based analogues (**4a-i**) against LYP.

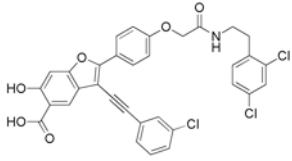
Cmpd #	R <sub>2</sub> =	<i>IC</i> <sub>50</sub> (μM)
<b>4a</b>	H	4.9 ± 0.3
<b>4b</b>	3-F	3.9 ± 0.2
<b>4c</b>	3-Cl	1.0 ± 0.07
<b>4d</b>	3-OCH <sub>3</sub>	17 ± 1
<b>4e</b>	2,4-di-F	3.5 ± 0.2
<b>4f</b>	3,5-di-F	1.3 ± 0.1
<b>4g</b>	3-CF <sub>3</sub>	2 ± 0.1
<b>4h</b>	4-OCF <sub>3</sub>	2 ± 0.1
<b>4i</b>	4-OC <sub>6</sub> H <sub>5</sub>	0.63 ± 0.03

**Table 3***IC*<sub>50</sub> of compounds **5a–d** against LYP.

Cmpd #	Structure	<i>IC</i> <sub>50</sub> (μM)
<b>5a</b>		0.68 ± 0.08
<b>5b</b>		0.61 ± 0.03
<b>5c</b>		2.1 ± 0.3
<b>5d</b>		2.5 ± 0.2

**Table 4***IC*<sub>50</sub> of the top eight hits from libraries **7** and **8** against LYP.

Cmpd #	Structure	<i>IC</i> <sub>50</sub> (μM)
<b>7a</b>		0.30 ± 0.009
<b>8a</b>		0.171 ± 0.004
<b>8b</b>		0.259 ± 0.007
<b>8c</b>		0.263 ± 0.006
<b>8d</b>		0.31 ± 0.008
<b>8e</b>		0.55 ± 0.03
<b>8f</b>		0.259 ± 0.008

Cmpd #	Structure	$IC_{50}$ ( $\mu$ M)
8g	 <p>The chemical structure of compound 8g is a complex molecule. It features a central benzofuran ring system. The furan oxygen is at the top. The benzene ring of the benzofuran has a hydroxyl group (-OH) at the 6-position and a carboxylic acid group (-COOH) at the 7-position. At the 2-position of the benzofuran, there is a propargyl group (-C≡C-CH<sub>2</sub>-) which is further substituted with a 4-chlorophenyl ring. At the 3-position of the benzofuran, there is a propyl chain (-CH<sub>2</sub>-CH<sub>2</sub>-CH<sub>2</sub>-) which is substituted with a 3,5-dichlorophenyl ring. The terminal carbon of the propyl chain is connected to a carbonyl group (-C(=O)-) which is part of an amide linkage (-NH-) to another propyl chain (-CH<sub>2</sub>-CH<sub>2</sub>-CH<sub>2</sub>-). This second propyl chain is substituted with a 4-chlorophenyl ring. The entire molecule is shown in a skeletal structure format.</p>	$0.67 \pm 0.03$

**Table 5***IC*<sub>50</sub> values of **8a** and **8b** against a panel of PTPs.

PTP	<i>IC</i> <sub>50</sub> (μM) for <b>8a</b>	<i>IC</i> <sub>50</sub> (μM) for <b>8b</b>
LYP	0.171 ± 0.004	0.259 ± 0.007
PTP1B	1.7 ± 0.4	10 ± 1
SHP1	0.91 ± 0.09	5 ± 0.5
SHP2	0.56 ± 0.03	2.5 ± 0.1
TC-PTP	11.3 ± 0.5	24 ± 1
HePTP	3 ± 0.6	15 ± 2
PTP-Meg2	0.59 ± 0.03	3 ± 0.3
FAP1	0.39 ± 0.02	2.9 ± 0.2
PTP-PEST	0.80 ± 0.10	2.4 ± 0.3
PTPH1	1.6 ± 0.6	13 ± 4
CD45	3.2 ± 0.6	12 ± 5
LAR	No inhibition at 100 μM	No inhibition at 100 μM
PTP $\alpha$	No inhibition at 100 μM	No inhibition at 100 μM
PTP $\beta$	0.47 ± 0.05	12 ± 5
PTP $\epsilon$	>25	>25
PTP $\gamma$	4 ± 2	15 ± 6
PTP $\mu$	7 ± 1	12 ± 2
PTP $\sigma$	No inhibition at 100 μM	No inhibition at 100 μM
Laforin	No inhibition at 100 μM	No inhibition at 100 μM
VHR	5.9 ± 0.5	14 ± 1
VHX	2.9 ± 0.6	4.6 ± 0.7
VHZ	3.4 ± 0.3	5.7 ± 0.7
MKP3	No inhibition at 100 μM	No inhibition at 100 μM
CDC14	30 ± 10	24 ± 2
LMWPTP	0.34 ± 0.07	7 ± 2

All measurements were made by using *p*NPP as a substrate at pH 7.0, 25°C, and ionic strength of 0.15 M.

Table 6

## Data collection and refinement statistics

	LYP•8b
Crystal parameters	
space group	$P2_12_12_1$
Cell Dimensions	
a (Å)	46.19
b (Å)	93.64
c (Å)	153.50
Data Collection	
resolution range (Å)	50.0 – 2.30
no. of unique reflections	28140
completeness (%)	93.3
redundancy	6.3
$R_{\text{merge}}^a$	0.065
Refinement	
resolution range (Å)	50.0 – 2.30
no. of reflections used ( $F$ 1.56 ( $F$ ))	26388
completeness (%)	86.7
no. of protein atoms	4998
no. of inhibitors	2
no. of waters	48
$R_{\text{work}}^b/R_{\text{free}}^c$	18.87/23.81
rms Deviations from Ideal Geometry	
bond length (Å)	0.010
bond angle (°)	1.42

$$^a R_{\text{merge}} = \frac{\sum_h \sum_i |I(h)_i - \langle I(h) \rangle|}{\sum_h \sum_i I(h)_i}$$

$^b R_{\text{work}} = \frac{\sum_h |F(h)_{\text{calcd}} - F(h)_{\text{obsd}}|}{\sum_h F(h)_{\text{obsd}}}$ , where  $F(h)_{\text{calcd}}$  and  $F(h)_{\text{obsd}}$  were the refined calculated and observed structure factors, respectively.

$^c R_{\text{free}}$  was calculated for a randomly selected 4.2% of the reflections that was omitted from refinement.